Published in final edited form as:
Nature. 2016 January 14; 529(7585): 216–220. doi:10.1038/nature16498.

FOXO1 couples metabolic activity and growth state in the vascular endothelium

Kerstin Wilhelm[1], **Katharina Happel**[1], **Guy Eelen**[2,3], **Sandra Schoors**[2,3], **Mark F. Oellerich**[1], **Radiance Lim**[1], **Barbara Zimmermann**[1], **Irene M. Aspalter**[4], **Claudio A. Franco**[5], **Thomas Boettger**[6], **Thomas Braun**[6], **Marcus Fruttiger**[7], **Klaus Rajewsky**[8], **Charles Keller**[9], **Jens C. Brüning**[10], **Holger Gerhardt**[4,11,12], **Peter Carmeliet**[2,3], and **Michael Potente**[1,*]

[1]Angiogenesis & Metabolism Laboratory, Max Planck Institute for Heart and Lung Research, D-61231 Bad Nauheim

[2]Laboratory of Angiogenesis and Neurovascular Link, Vesalius Research Center, Department of Oncology, University of Leuven, Leuven 3000, Belgium

[3]Laboratory of Angiogenesis and Neurovascular Link, Vesalius Research Center, VIB, Leuven 3000, Belgium

[4]Vascular Biology Laboratory, London Research Institute, Cancer Research UK, London WC2A 3LY, UK

[5]Vascular Morphogenesis Laboratory, Instituto de Medicina Molecular, Faculdade de Medicina Universidade de Lisboa, Lisboa 1649-028, Portugal

[6]Department of Cardiac Development and Remodeling, Max Planck Institute for Heart and Lung Research, D-61231 Bad Nauheim

[7]UCL Institute of Ophthalmology, University College London, London EC1V 9EL, UK

[8]Immune Regulation and Cancer, Max Delbrück Center for Molecular Medicine (MDC), D-13125 Berlin, Germany

[9]Children's Cancer Therapy Development Institute, Fort Collins, CO 80524, USA

[10]Max Planck Institute for Neurological Research, Excellence Cluster on Cellular Stress Responses in Aging-Associated Diseases (CECAD) and Center of Molecular Medicine Cologne

[*]**Editorial correspondence:** Michael Potente, M.D. Angiogenesis & Metabolism Laboratory Max Planck Institute for Heart and Lung Research Ludwigstr. 43 D-61231 Bad Nauheim Germany Phone: +49 6032 705 1107 Fax: +49 6032 705 1104 michael.potente@mpi-bn.mpg.de.

Author Contributions

K.W., K.H., G.E., S.S., M.F.O., R.L., B.Z., I.M.A., C.A.F., T.Bo., and M.P. performed experiments. K.W., K.H., G.E., S.S., M.F.O., R.L., B.Z., I.M.A., C.A.F., T.Bo., H.G., P.C., and M.P. analysed data. H.G., P.C., and M.P. guided research. T.Br., M.F., K.R., C.K., J.C.B., and H.G. provided essential reagents and protocols. K.H. contributed to manuscript writing and preparation. K.W., H.G., P.C., and M.P. wrote the paper. M.P. conceived and directed the study. All authors discussed the results and commented on the manuscript.

Data from microarray analysis have been deposited in the ArrayExpress repository under the accessions E-MTAB-4023 and E-MTAB-4025.

The authors declare no competing financial interests.

Europe PMC Funders Author Manuscripts

(CMMC), Center for Endocrinology, Diabetes and Preventive Medicine (CEDP), Institute for Genetics, University of Cologne, D-50931 Cologne, Germany

[11]Vascular Patterning Laboratory, Vesalius Research Center, VIB and University of Leuven, Leuven 3000, Belgium

[12]Max Delbrück Center for Molecular Medicine (MDC), D-12125 Berlin, Germany

Abstract

Endothelial cells (ECs) are plastic cells that can switch between growth states with different bioenergetic and biosynthetic requirements[1]. Although quiescent in most healthy tissues, ECs divide and migrate rapidly upon proangiogenic stimulation[2,3]. Adjusting endothelial metabolism to growth state is central to normal vessel growth and function[1,4], yet poorly understood at the molecular level. Here we report that the forkhead box O (FOXO) transcription factor FOXO1 is an essential regulator of vascular growth that couples metabolic and proliferative activities in ECs. Endothelial-restricted deletion of FOXO1 in mice induces a profound increase in EC proliferation that interferes with coordinated sprouting, thereby causing hyperplasia and vessel enlargement. Conversely, forced expression of FOXO1 restricts vascular expansion and leads to vessel thinning and hypobranching. We find that FOXO1 acts as a gatekeeper of endothelial quiescence, which decelerates metabolic activity by reducing glycolysis and mitochondrial respiration. Mechanistically, FOXO1 suppresses signalling by c-MYC (termed MYC hereafter), a powerful driver of anabolic metabolism and growth[5,6]. MYC ablation impairs glycolysis, mitochondrial function and proliferation of ECs while its EC-specific overexpression fuels these processes. Moreover, restoration of MYC signalling in FOXO1-overexpressing endothelium normalises metabolic activity and branching behaviour. Our findings identify FOXO1 as a critical rheostat of vascular expansion and define the FOXO1 – MYC transcriptional network as a novel metabolic checkpoint during endothelial growth and proliferation.

FOXOs are effectors of the phosphoinositide 3-kinase (PI3K) / AKT pathway that links growth and metabolism[7,8]. PI3K signalling inhibits FOXOs through AKT-mediated phosphorylation leading to their nuclear exclusion[9,10]. We investigated the role of FOXO1 in ECs, an enriched FOXO family member in the endothelium[11-15]. To this end, we bred floxed *Foxo1* mice (*Foxo1*^{flox})[16] with a *Tie2-Cre deleter* (Extended Data Fig. 1a), which recombines in endothelial and hematopoietic cells. *Tie2-Cre*-mediated deletion of *Foxo1* (*Foxo1*$^{EC\text{-}KO}$) caused defective vascular development and embryonic lethality around E10.5[17] (Extended Data Fig. 1b,c), suggesting that endothelial FOXO1 is essential for embryo development.

Immunofluorescence analysis of developing blood vessels in the postnatal retina showed high levels of FOXO1 expression in the endothelium (Fig. 1a). Further examination of the subcellular distribution revealed a diffuse nucleo-cytoplasmic localization of FOXO1 at the angiogenic front, where most of the EC proliferation occurs, but a stronger nuclear pattern in the plexus, where vessels remodel, and endothelial proliferation abates (Fig. 1a). This spatial difference in subcellular localization suggests that FOXO1 is important for governing endothelial growth. To test this, we assessed the impact of *Foxo1* deletion on retinal angiogenesis using the tamoxifen-inducible, endothelial-selective *Pdgfb-CreERT2* line

(*Foxo1*$^{iEC\text{-}KO}$). Recombination was monitored with the *Rosa26-mT/mG* (*mTmG*) reporter that expresses GFP upon Cre-mediated recombination. 4-hydroxy-tamoxifen- (4-OHT) treatment resulted in broad GFP expression in ECs as well as extinction of endothelial FOXO1 staining (Extended Data Fig. 1d-f). Endothelial loss of *Foxo1* caused a dense and hyperplastic vasculature and resulted in the inability of ECs to extend proper sprouts (Fig. 1b-f). Instead, ECs grew in clusters leading to vessel enlargement and blunting of the angiogenic front (Fig. 1d,f). Strikingly, numerous filopodial bursts were emanating from the stunted front (Fig. 1c,d), suggesting that FOXO1 deficiency results in uncoordinated vascular growth. Staining *Foxo1*$^{iEC\text{-}KO}$ retinas for ERG (marking endothelial nuclei) and VE-cadherin (marking endothelial junctions), revealed an abundance of abnormally aligned ECs, which formed vessels with wide and irregular lumens (Extended Data Fig. 2a-c). Assessment of 5-bromo-2′-deoxyuridine (BrdU) incorporation and phospho-histone H3 (pHH3) labelling demonstrated a substantial increase in endothelial proliferation in the *Foxo1*$^{iEC\text{-}KO}$ mutants (Fig. 1g,j and Extended Data Fig. 2d), indicating that deregulated proliferation drives this aberrant vessel phenotype. Importantly, the vascular defects of the *Foxo1*$^{iEC\text{-}KO}$ mice did not normalize at later stages of development, but showed a persistent increase in endothelial number, density and vessel diameter (Fig. 1h,i and Extended Data Fig. 2e-g). We conclude that FOXO1 is a suppressor of endothelial growth and proliferation, whose inactivation leads to uncontrolled overgrowth.

Next, we determined the consequences of FOXO1 activation in ECs. We used a Cre-inducible gain-of-function allele (*Foxo1*^{CA}) in which the AKT phosphorylation sites are mutated, thus, rendering FOXO1 constitutively nuclear (Extended Data Fig. 3a)[18]. *Tie2-Cre*-mediated expression of this IRES-GFP coexpressing mutant (*Foxo1*$^{EC\text{-}CA}$) was incompatible with embryo survival beyond E10.5 (Fig. 2a), highlighting the sensitivity of ECs towards changes in FOXO1 status. We then used the *Pdgfb-CreERT2* strain to express *Foxo1*^{CA} in the retinal endothelium (*Foxo1*$^{iEC\text{-}CA}$). Immunofluorescence studies revealed an enriched FOXO1 signal in endothelial nuclei and confirmed the EC-specific expression of GFP (Fig. 2b and Extended Data Fig. 3b,c,g). Forced activation of FOXO1 led to a sparse and hyperpruned vascular network that contained less ECs (Fig. 2c,d,f-h and Extended Data Fig. 3g). These retinal vessels established a lumen but were thinner and extended fewer filopodia (Fig. 2g,h and Extended Data Fig. 3d). Staining for BrdU-incorporation and pHH3 revealed a reduction in EC proliferation in *Foxo1*$^{iEC\text{-}CA}$ mice while endothelial apoptosis was not altered (Fig. 2e,f,i and Extended Data Fig. 3e,g). Similar phenotypes were observed in the hindbrain vasculature (Fig. 2j,k and Extended Data Fig. 4a-c), indicating that FOXO1 is a critical driver of endothelial quiescence. To further examine this, we analysed mosaic retinas of *mTmG* coexpressing control- and *Foxo1*$^{iEC\text{-}CA}$ mice, in which the majority of ECs are un-recombined. Compared to controls, *Foxo1*$^{iEC\text{-}CA}$ mice showed an impaired propagation of GFP-positive ECs in the retinal plexus (Extended Data Fig. 4d-f), arguing that the proquiescent activity of FOXO1 is cell-autonomous.

We next assessed whether FOXO1 regulates endothelial metabolism. Since ECs rely on glycolysis for vessel branching[4], we first studied the effects of FOXO1 on this metabolic pathway. Transduction of human umbilical vein endothelial cells (HUVECs) with a FOXO1^{CA}-encoding adenovirus (AdFOXO1^{CA}) led to a robust reduction in glycolysis as evidenced by a reduction in extracellular acidification rate (ECAR), glucose uptake,

glycolytic flux and lactate production (Fig. 3a-d and Extended Data Fig. 5a). This metabolic phenotype correlates with the reduced proliferation in FOXO1^{CA}-expressing ECs and raises the question whether FOXO1 promotes mitochondrial oxidative phosphorylation. Surprisingly, FOXO1 did not stimulate but instead diminished oxidative metabolism as indicated by a decline in oxygen consumption in AdFOXO1^{CA}-expressing HUVECs (Fig. 3e). Moreover, reactive oxygen species (ROS) formation and ATP levels were decreased (Fig. 3f and Extended Data Fig. 5b). Importantly, FOXO1 did not induce endothelial apoptosis, senescence, autophagy or energy distress under the same experimental conditions (Fig. 3g and Extended Data Fig. 5c-h). Together, our data indicate that FOXO1 adapts metabolic activity to the lower requirements of the quiescent endothelium.

To gain insight into the underlying mechanisms, we performed transcriptome analysis of FOXO1^{CA}- and GFP-transduced HUVECs. Gene set enrichment analysis (GSEA) revealed an enrichment of the FOXO1 DNA-binding elements in genes induced by FOXO1, while the MYC DNA-binding motif was highly enriched in the repressed genes (Fig. 3h and Extended Data Fig. 6a,b). Moreover, MYC target gene signatures were downregulated in the FOXO1 transcriptome (Fig. 3i and Extended Data Fig. 6c). Since MYC is a powerful driver of glycolysis, mitochondrial metabolism and growth[5], FOXO1 might antagonize endothelial MYC signalling. In line with this, overexpression of FOXO1^{CA} suppressed MYC expression, whereas FOXO1 depletion enhanced MYC levels, both in HUVECs and in ECs derived from the mutant mice (Fig. 3j-l and Extended Data Fig. 6d-h). Immunofluorescence studies in *Foxo1*$^{iEC\text{-}CA}$ retinas confirmed these findings and showed a suppression of endothelial MYC expression (Extended Data Fig. 3f). Accordingly, numerous genes that are induced by MYC were downregulated in FOXO1^{CA}-overexpressing HUVECs including genes involved in cell metabolism and cell-cycle progression (Fig. 3i,l). This regulation is in line with the repression of MYC by FOXOs in cancer cells[19-23] and points to MYC as a crucial effector of FOXO1 in the coordination of endothelial metabolism and growth.

Remarkably, FOXO1 also induced the expression of negative regulators of MYC signalling including *MXI1*, an antagonist of MYC transcriptional activity[6], and *FBXW7*, an E3 ubiquitin ligase that targets MYC for proteasomal degradation[6] (Fig. 3l and Extended Data Fig. 7a). Consistent with these findings, MYC protein stability was decreased in FOXO1^{CA}-expressing ECs and co-treatment with the proteasomal inhibitor MG132 partially restored MYC protein levels (Extended Data Fig. 7b,c). Knockdown of MXI1, on the other hand, did not affect the FOXO1-induced repression of MYC but attenuated the ability of FOXO1 to downregulate MYC target genes (Extended Data Fig. 7d-f). These data are in accordance with the function of MXI1 as a negative regulator of MYC activity[6,19,20], and suggest that FOXO1 intersects with MYC signalling at different levels.

To further explore the role of MYC in ECs, we profiled the transcriptome of MYC siRNA-transfected (siMYC) HUVECs. This analysis showed a suppression of MYC signature genes involved in metabolic processes and cell cycle progression and validated the regulation of predicted MYC targets that were repressed by FOXO1 (Extended Data Fig. 8a-g). Bioenergetic analysis revealed that MYC deficiency attenuated glycolysis and mitochondrial respiration, whereas adenoviral overexpression of MYC (AdMYC) stimulated these metabolic activities (Fig. 4a,b and Extended Data Fig. 9e). Conditional deletion of *Myc*

(*Myc*^{flox})[24] in mice using the *Pdgfb-CreERT2* deleter impaired vascular expansion and led to a thinned and poorly branched vasculature with reduced EC proliferation (Fig. 4c-e and Extended Data Fig. 9a-d). These phenotypes resemble the vascular defects in *Foxo1*$^{iEC\text{-}CA}$ mutant mice and imply that MYC is a central component of endothelial FOXO1 signalling. To test this directly, we attempted to rescue the endothelial phenotypes imposed by FOXO1 activation by restoring MYC signalling with a Cre-inducible *Myc* overexpressor allele (*Myc*^{OE})[25]. *Pdgfb-creERT2*-induced overexpression of MYC caused sustained vascular overgrowth and led to a profound increase in EC number, proliferation and vessel density (Fig. 4f,g and Extended Data Fig. 9f-k). We then combined *the Myc*^{OE}, *Foxo1*^{CA} and *Pdgfb-creERT2* alleles to generate endothelial-specific double mutants. Remarkably, reexpression of MYC in ECs of *Foxo1*$^{iEC\text{-}CA}$ mice normalized the hypobranched and hypocellular vascular phenotype caused by FOXO1 activation (Fig. 4h,i and Extended Data Fig. 10a,b). Moreover, coexpression of MYC and FOXO1^{CA} in HUVECs restored glycolysis, mitochondrial respiration and ROS formation (Fig. 4j,k and Extended Data Fig S10c), indicating that regulation of MYC signalling by FOXO1 is critical for the coordination of endothelial metabolism and growth.

This study identifies FOXO1 as a critical checkpoint of endothelial growth that restricts vascular expansion. Our data suggest that FOXO1 promotes endothelial quiescence by antagonizing MYC, which leads to a coordinated reduction in the proliferative and metabolic activity of ECs. The FOXO1-induced deceleration of metabolic activity might not only enforce quiescence but also support endothelial function. For instance, by lowering metabolism, ECs will consume less energetic fuel for their homeostatic needs, thereby ensuring efficient nutrient and oxygen delivery. Reducing metabolic activity might also contribute to endothelial redox balance. ECs are long-lived cells that need to protect themselves against oxidative damage exerted by high oxygen levels in the bloodstream. The FOXO1-induced reduction in oxidative metabolism might thus be a mechanism to minimize the production of mitochondria-derived ROS, thereby conferring protection against the high-oxygen environment. Such a role of FOXO1 in endothelial metabolism aligns with the broader function of FOXOs in mediating oxidative stress resistance[26-30], and might also explain why ECs are exquisitely sensitive to a change in FOXO1 status. It will now be interesting to determine how endothelial FOXO1 is regulated *in vivo* and how deregulation contributes to disease.

Methods

Animals and genetic experiments

All conditional *Foxo1* and *Myc* mutant mice were on a C57BL/6 genetic background and generated as described[16,18,24,25]. For constitutive Cre-mediated recombination in ECs, *Foxo1*^{flox} or *Rosa26-Foxo1*^{CA} mice were bred with *Tie2-Cre* transgenic mice[31]. To avoid recombination in the female germline, only *Tie2-Cre*-positive male mice were used for intercrossing. Embryos were collected from *Cre*-negative females at the indicated time points and genotyping performed from isolated yolk sacs. For inducible Cre-mediated recombination in ECs, floxed mice were bred with transgenic mice expressing the tamoxifen-inducible, *Pdgfb* promoter-driven *CreERT2*[32]. The degree of Cre-mediated

recombination was assessed with the double fluorescent Cre-reporter *Rosa26-mT/mG*[33] allele, which was crossed into the respective mutant mice. For the analysis of angiogenesis in the postnatal mouse retina, Cre-mediated recombination was induced in newborn mice by intraperitoneal (i.p.) injections of 25 µl 4-hydroxy-tamoxifen (4-OHT; 2 mg/ml; Sigma-Adrich) from postnatal day (P)1 – P4. Eyes were harvested at P5 or P21 for further analysis. In mosaic recombination experiments, 4-OHT (20 µl/g body weight of 0.02 mg/ml) was intraperitoneally injected at P3 and eyes collected at P5. To induce Cre-mediated recombination in mouse embryos, 100 µl of 4-OHT (10 mg/ml) was injected i.p. into pregnant females from embryonic day (E)8.5 – E10.5. Embryos were harvested at E11.5 for the analysis of angiogenesis in the embryonic hindbrain. The *Rosa26-Foxo1*^{CA}, *Rosa26-Myc, and Rosa26-mT/mG alleles* were kept heterozygous for the respective transgene in all experimental studies. Apart from the mosaic studies, control animals were littermate animals without *Cre* expression. Male and female mice were used for the analysis, which were maintained under specific pathogen-free conditions. Experiments involving animals were conducted in accordance with institutional guidelines and laws, following protocols approved by local animal ethics committees and authorities (Regierungspraesidium Darmstadt).

Immunohistochemistry of mouse tissues

To analyse blood vessel growth in the postnatal retina, whole mouse eyes were fixed in 4% paraformaldehyde (PFA) on ice for 1 hour. Eyes were washed in phosphate-buffered saline (PBS) before the retinas were dissected and partially cut into 4 leaflets. After blocking / permeabilization in 2% goat-serum (Vector labs), 1% BSA and 0.5% Triton X-100 (in PBS) for 1 hour at room temperature, the retinas were incubated at 4°C overnight in incubation buffer containing 1% goat-serum, 0.5% BSA and 0.25% Triton X-100 (in PBS) and the primary antibody. Primary antibodies against the following proteins were used: cleaved Caspase 3 (Cell Signaling Technology, #9664, 1:100), Collagen IV (AbD Serotec, #2150-1470, 1:400), ERG 1/2/3 (Abcam, #ab92513, 1:200), FOXO1 (Cell Signaling Technology, #2880, 1:100), GFP (Invitrogen, #A21311, 1:100), ICAM2 (BD Biosciences, #553326, 1:200), MYC (Millipore, 06-340, 1:100), PECAM-1 (R&D Systems, AF3628, 1:400), phospho-histone H3 (Chemicon, #06-570, 1:100), TER119 (BD Biosciences, #553670, 1:100), and VE-Cadherin (BD Biosciences, #555289, 1:25). After 4 washes with 0.1% Triton X-100 in PBS (PBST), retinas were incubated with Alexa-Fluor 488-, Alexa-Fluor 555- or Alexa-Fluor 647-conjugated secondary antibodies (Invitrogen, 1:400) for 2 hours at room temperature. For staining ECs with isolectin B4 (iB4), retinas were washed with PBLEC buffer (1 mM $CaCl_2$, 1 mM $MgCl_2$, 1 mM $MnCl_2$ and 1% Triton X-100 in PBS) and incubated with biotinylated iB4 (*Griffonia simplicifolia*, #B1205, Vector labs, 1:100) diluted in PBLEC buffer. After washing, retinas were incubated in Alexa-Fluor-coupled streptavidin (Invitrogen, #S21374, 1:200) for 2 h at room temperature. For nuclear counterstain, retinas were incubated with DAPI (Sigma Aldrich, #D9542, 1:1000) for 15 min following washes with PBST and PBS. The labelling of proliferating cells with 5-bromo-2′ deoxyuridine (BrdU) was performed in P5 pups. In brief, 50 mg/kg of BrdU (Invitrogen, #B23151) per pup was injected intraperitoneally 3 h before they were sacrificed. Retinas were fixed for 2 h in 4% PFA and then incubated for 1 h in 65°C warm formamide, followed by an incubation of 30 min in 2N HCl. Afterwards retinas were washed twice with

0.1M Tris-HCl (pH8) and then blocked in 1% BSA, 0.5% Tween 20 in PBS and incubated overnight at 4°C with a mouse anti-BrdU antibody (BD Biosciences, #347580, 1:50). The detection was performed with Alexa Fluor-488 anti-mouse secondary antibody (Invitrogen, A21202, 1:400). After the BrdU staining, retinas were processed for the iB4 staining as described above. The dissection of the embryonic hindbrain was performed as described[34]. Following overnight fixation in 4% PFA, dissected hindbrains were incubated in a blocking solution containing 10% serum, 1% BSA and 0.5% Triton X-100 in PBS at 4°C. After washes with PBS, hindbrains were incubated for 1 h in PBLEC buffer prior to the overnight incubation with Alexa Fluor-conjugated iB4 (Invitrogen, #I21411, 1:100 in PBLEC) at 4°C. Hindbrains were washed with PBS and stained with DAPI. Retinas and embryonic hindbrains were flat-mounted with Vectashield (Vector labs) and examined by confocal laser microscopy (Leica TCS SP5 or SP8). Immunostainings were carried out in tissues from littermates and processed under the same conditions.

Immunohistochemistry of cell cultures

HUVECs were seeded on glass bottom culture dishes (Mattek) and cultured at 37°C and 5% CO_2. To detect autophagy, cells were washed and fixed with 4% PFA for 20 min at room temperature. Permeabilisation was performed in 1% BSA, 10% donkey serum and 0.5% Tween-20 in PBS. Cells were stained for anti-LC3A/B (Cell signaling Technology, #12741, 1:400), Phalloidin-TRITC (Sigma Aldrich, #P1951, 1:500) and DAPI in incubation buffer (0.5% BSA, 5% donkey serum and 0.25% Tween-20 in PBS). Following washes with PBST, samples were incubated with AlexaFluor-conjugated secondary antibodies (Invitrogen, 1:200). Cells were washed and mounted in VectaShield. As a positive control, HUVECs were treated with 50 μM Chloroquine overnight prior to fixation.

Image acquisition and processing

Stained tissue / cells were analysed at high resolution with a TCS SP8 confocal microscope (Leica). Volocity (Perkin Elmer), Fiji / ImageJ, Photoshop (Adobe) and Adobe Illustrator (Adobe) software were used for image acquisition and processing. For all of the images in which the levels of immunostaining were compared, settings for laser excitation and confocal scanner detection were kept constant between groups.

Quantitative analysis of the retinal and hindbrain vasculature

All quantifications were done on high-resolution confocal images of thin z sections of the sample using the Volocity (Perkin Elmer) software. In the retina, endothelial coverage, the number of endothelial branchpoints, and the average vessel branch diameter were quantified behind the angiogenic front in a region between an artery and a vein. In the embryonic hindbrain, randomly chosen fields were used to quantify the vascularization in the ventricular zone. All parameters were quantified in a minimum of four vascularized fields per sample. Endothelial coverage was determined by assessing the ratio of the iB4-positive area to the total area of the vascularized field (sized 200 μm × 200 μm), and expressed as percentage of the area covered by iB4-positive ECs. Average vessel diameter was analysed by assessing the diameter of individual vessel branches in a vascularized field (sized 200 μm × 200 μm), which was used to calculate the mean diameter in each field. The diameter of individual vessel branches was averaged from three measurements taken at the proximal,

middle and distal part of the vessel segment. The number of filopodial extensions was quantified at the angiogenic front. The total number of filopodia was normalized to a vessel length of 100 μm at the angiogenic front, which was defined and measured according to published protocols[35]. For quantifying vascular outgrowth in the mouse retina, the distance of vessel growth from the centre of the optic nerve to the periphery was measured in each leaflet of a dissected retina, which was used to calculate the mean value for each sample. The number of ERG-/iB4- and BrdU-/iB4-labelled cells was counted in at least 4 fields sized 200 μm × 200 μm per sample. Because of the lower incidence of pHH3-positive ECs, the number of pHH3-/iB4- double-positive cells was quantified in larger fields (sized 580 μm × 580 μm). For the quantification of the mosaic control (*Pdgfb-CreERT2;Rosa26-Foxo1+/+;Rosa26-mTmG*$^{flox/+}$) and *Foxo1*$^{iEC\text{-}CA}$ (*Pdgfb-CreERT2;Rosa26-Foxo1*$^{CA/+}$*;Rosa26-mTmG*$^{flox/+}$) retinas, the GFP/IB4 double-positive area per field was determined and divided by the total IB4-positive area. The percentage of the GFP/IB4 double-positive area per total IB4 area was measured in 4 fields (400 μm × 400 μm) per sample and used to calculate the mean value. For the quantification of nuclear FOXO1 expression in control and *Foxo1*$^{iEC\text{-}CA}$ mice, high-resolution confocal images were taken with a 40x objective. The resulting images were analysed with the Bitplane Imaris software. Vessels were first segmented using the Surface module in Imaris. FOXO1 immunofluorescence was then used to set a threshold in the new vascular surface area, in which only CD31-positive nuclei were selected (Surface module). The sum intensity of the nuclear FOXO1 fluorescence was divided by the total vascular area to adjust for differences in vascular density on each image. An average of 6 images per sample was quantified in 3 animals per group. All of the images shown are representative of the vascular phenotype observed in samples from at least two distinct litters per group.

Cell culture

Pooled human umbilical vein endothelial cells (HUVECs) were purchased from Lonza and authenticated by marker expression (CD31/CD105 double-positive) and morphology. HUVECs were cultured in endothelial basal medium (EBM, Lonza) supplemented with hydrocortisone (1 μg/ml), bovine brain extract (12 μg/ml), gentamicin (50 μg/ml), amphotericin B (50 ng/ml), epidermal growth factor (10 ng/ml), and 10% fetal bovine serum (FBS, Life Technologies). HUVECs were tested negative for mycoplasma and cultured until the fourth passage. The isolation of mouse lung ECs was performed as described[36]. In brief, adult mice were sacrificed, lungs removed, and incubated with dispase. The homogenate was filtered through a cell strainer, collected by centrifugation, and washed with PBS containing 0.1% BSA (PBSB). The resulting cell suspension was incubated with rat anti-mouse VE-Cadherin antibody- (BD Pharmingen, #555289) coated magnetic beads (Dynabeads, Invitrogen, #11035). Next, the beads were washed with PBSB and then re-suspended in D-MEM/F12 (Invitrogen) supplemented with 20% FCS, endothelial growth factor (Promocell, #c-30140), penicillin and streptomycin. The isolated cells were seeded on gelatin-coated culture dishes and re-purified with the VE-Cadherin antibody during the first three passages.

Adenoviral infection

Sub-confluent HUVECs were infected with adenoviruses to overexpress constitutively active human FOXO1-Flag (FOXO1^{CA})[37], human c-MYC-HA[38] (Vector Biolabs) and GFP or

LacZ as a control. HUVECs (70–80% confluent) were incubated in EBM containing 0.1% BSA for 4 h. Prior to infection, adenoviruses were incubated with an antennapedia-derived peptide (Eurogentec) to facilitate the infection. The mixture was then applied to the HUVECs cultured in EBM containing 0.1% BSA and incubated for 4 h. Thereafter, the cells were washed five times and cultured in EBM with 10% FCS and supplements. The adenoviral infection of murine ECs was performed with adenoviruses encoding for Cre or GFP (Vector Biolabs) as a control.

RNA interference

To silence FOXO1, MYC or MXI1 gene expression, HUVECs were transfected with a pool of siRNA duplexes directed against human FOXO1, human c-MYC or human MXI1 (ON-TARGETplus SMARTpool, Dharmacon). A negative control pool of four siRNAs designed and microarray-tested for minimal targeting of human, mouse or rat genes was used as a control (ON-TARGETplus Non-targeting pool, Dharmacon). HUVECs were transfected with 50 nM of the indicated siRNAs using Lipofectamine RNAiMAX (Invitrogen) according to the manufacturer's recommendations.

Microarray and gene set enrichment analysis

Total RNA quality was verified using the Agilent Bioanalyser and the 6000 nano kit. RNA was labelled according to the Affymetrix Whole Transcript Sense Target Labelling protocol. Affymetrix GeneChip Human Gene 1.0 ST arrays were hybridized, processed and scanned using the appropriate Affymetrix protocols. Data were analysed using the Affymetrix expression console using the RMA algorithm, statistical analysis was done using DNAStar Arraystar 11. Heat maps were generated using GENE-E, publicly available from the Broad Institute (http://www.broadinstitute.org/cancer/software/GENE-E/). For Gene Set Enrichment Analysis (GSEA), gene set collections from the Molecular Signatures Database (MSigDB) 4.0 (http://www.broadinstitute.org/gsea/msigdb/) were used for the analysis of the endothelial FOXO1 and MYC transcriptomes.

RNA extraction and quantitative realtime-PCR (qRT-PCR)

RNA was extracted from cells using the RNeasy Mini Kit (Qiagen) according to the manufacturer's instructions. cDNA synthesis was performed on 2 μg of total RNA using the M-MLV reverse transcriptase (Invitrogen). qPCR was performed with TaqMan Gene Expression Master Mix (Applied Biosystems) and TaqMan probes (TaqMan Gene Expression Assays) available from Applied Biosystems. TaqMan Gene Expression Assays used were as follows: human *ACTB* Hs99999903_m1; *CCNB2* Hs00270424_m1; *CCND1* Hs00765553_m1; *CCND2* Hs00153380_m1; *CDK4* Hs00262861_m1; *c-MYC* Hs00153408_m1; *ENO1* Hs00361415_m1; *FASN* Hs01005622_m1; *FBXW7* Hs00217794_m1; *FOXO1* Hs01054576_m1; *LDHA* Hs00855332_g1; *LDHB* Hs00929956_m1; *MXI1* Hs00365651_m1; *PKM2* Hs00987254_m1. Mouse probes were: *Actb* Mm 00607939_s1; *Myc* Mm00487804_m1. All qPCR reactions were run on a StepOnePlus real-time PCR instrument (Applied Biosystems) and data were calculated using the $\Delta\Delta Ct$ method.

Western blot analysis and antibodies

Western blot analyses were performed with precast gradient gels (Bio-Rad) using standard methods. Briefly, HUVECs were lysed in RIPA buffer (150 mM NaCl, 1.0% IGEPAL CA-630, 0.5% sodium deoxycholate, 0.1% SDS, and 50 mM Tris, pH 8.0) supplemented with a protease inhibitor mix (Complete Mini Protease Inhibitor cocktail tablets, Roche) and phenylmethylsulfonyl fluoride. Proteins were separated by SDS-PAGE and blotted onto nitrocellulose membranes (Bio-Rad). Membranes were probed with specific primary antibodies and then with peroxidase-conjugated secondary antibodies. The following antibodies were used: AMPKα (Cell Signaling Technology, #2532, 1:1000), Caspase 3 (Cell Signaling Technology, #9662, 1:1000), cleaved Caspase 3 (Asp175) (Cell Signaling Technology, #9664, 1:1000), cleaved PARP (Cell Signaling Technology, #5625, 1:1000), c-MYC (Cell Signaling Technology, #9402, 1:1000), FBXW7 (Abcam, #12292, 1:500), Flag M2 (Sigma, #F-3165, 1:1000), FOXO1 (Cell Signaling Technology, #2880, 1:1000), HA (Covance, clone 16B12, MMS-101P), 1:1000), LC3A/B (Cell Signaling Technology, #12741, 1:1000), MXI1 (Santa Cruz, SC-1042, 1:500), P-ACC (Cell Signaling Technology, #3661, 1:1000), P-AMPKα (Thr172) (Cell Signaling Technology, #2535, 1:1000), PARP (Cell Signaling Technology, #9532, 1:1000), Tubulin (Cell Signaling Technology, #2148, 1:1000). The bands were visualised by chemiluminescence using an ECL detection kit (Clarity Western ECL Substrate, Bio-Rad) and a ChemiDoc MP Imaging System (Bio-Rad). The gel source data of the Western blot analysis is illustrated in Supplementary Figure 1. Quantification of band intensities by densitometry was carried out using the Image Lab software (Bio-Rad).

Metabolic Assays

Extracellular acidification (ECAR) and oxygen consumption (OCR) rates were measured using the Seahorse XFe96 analyzer (Seahorse Bioscience) following the manufacturer's protocols. Briefly, ECAR and OCR were measured 4 h after seeding HUVECs (40.000 cells per well) on fibronectin-coated XFe96 microplates. HUVECs were maintained in non-buffered assay medium in a non-CO_2 incubator for 1 h before the assay. The Glycolysis stress test kit (Seahorse Bioscience) was used to monitor the extracellular acidification rate under various conditions. Three baseline recordings were made, followed by sequential injection of glucose (10 mM), the mitochondrial / ATP synthase inhibitor oligomycin (3 μM), and the glycolysis inhibitor 2-deoxy-D-glucose (2-DG; 100 mM). The Mito stress test kit was used to assay the mitochondrial respiration rate under basal conditions, in the presence of the ATP synthase inhibitor oligomycin (3 μM), the mitochondrial uncoupler carbonyl cyanide-4-(trifluoromethoxy)phenyl-hydrazone (FCCP; 1 μM), and the respiratory chain inhibitors antimycin A (1.5 μM) and rotenone (3 μM). To measure glycolysis in ECs, HUVECs were incubated for 2 hours in growth medium containing 80 mCi/mmol [5-^{3}H]-D-glucose (Perkin Elmer). Thereafter, supernatant was transferred into glass vials sealed with rubber stoppers. ^3H_2O was captured in hanging wells containing a Whatman paper soaked with H_2O over a period of 48 hours at 37°C to reach saturation[4]. Radioactivity was determined by liquid scintillation counting and normalized to protein content. Lactate concentration in the HUVEC culture media was measured by using a Lactate assay kit (Biovision) following the instructions of the manufacturer. Glucose uptake was assessed by analysing the uptake of 2-deoxyglucose (2-DG) with a Colorimetric Assay (BioVision). ATP

was measured from lysates from HUVECs (1×10^6/ml) with an ATP Bioluminescence Assay Kit CLS II (Roche) according to the instructions of the manufacturer.

Intracellular ROS measurement

Intracellular ROS levels were determined using CM-H_2DCFDA dye (Life technologies). Dye was reconstituted in DMSO (10mM) and diluted 1:1000 in PBS containing $CaCl_2$ and $MagCl_2$ as working solution. 24 hours post transduction, 1×10^6 cells were incubated in 1 ml working solution for 40 min at 37°C in the dark. Subsequently fluorescence of 10,000 living endothelial cells per sample was measured at the BD FACS LSR II flow cytometer. The assays were performed with adenoviruses, which did not co-express fluorescent reporter genes. Data were analysed using BD FACSDiva software (Version 8.0.1).

Senescence-associated β-galactosidase staining

To detect senescence-associated β-galactosidase activity in HUVECs, a cellular senescence assay kit (#KAA002, Chemicon) was used according to the manufacturer's instructions. Briefly, cells were fixed in 1 ml Fixing Solution at room temperature for 15 min. 2 ml of freshly prepared SA-β-gal Detection Solution was added and cells were incubated overnight at 37°C without CO_2 and protected from light. Then Detection solution was removed and cells were washed and mounted in 70% glycerol in PBS. H_2O_2-treated HUVECs were used as a positive control.

Statistical analysis

Statistical analysis was performed by unpaired, two-tailed Student's *t*-test, or non-parametric one-way ANOVA followed by Bonferroni's multiple comparison test unless mentioned otherwise. For all bar graphs, data are represented as mean ± s.d. *P* values < 0.05 were considered significant. All calculations were performed using GraphPad Prism software. No randomization or blinding was used and no animals were excluded from the analysis. Sample sizes were selected on the basis of published protocols[34,35] and previous experiments. Several independent experiments were performed to guarantee reproducibility and robustness of findings.

Europe PMC Funders Author Manuscripts

Extended Data

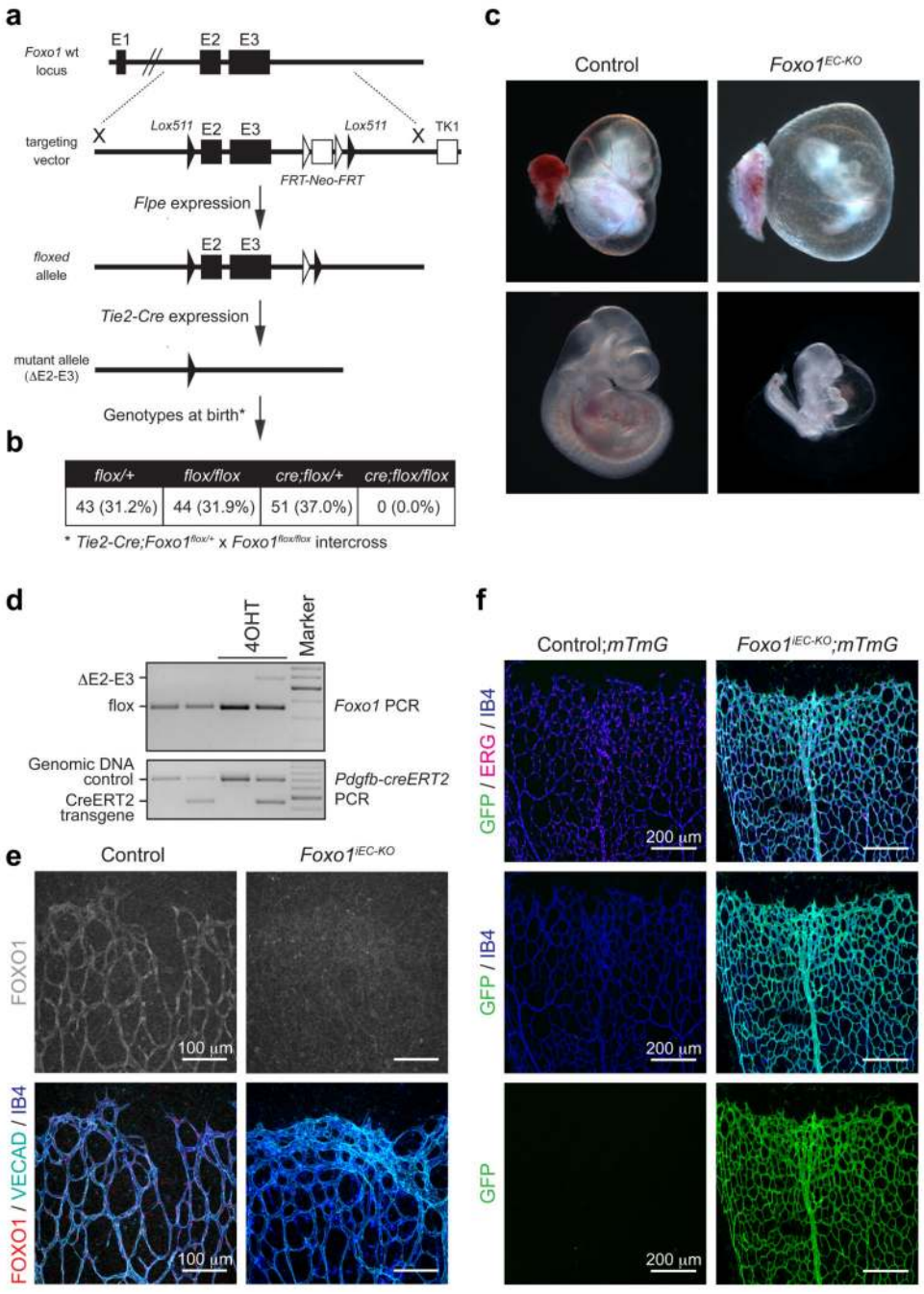

Extended Data Figure 1. Constitutive and inducible deletion of *Foxo1* in ECs of mice

a, Strategy to generate a conditional *Foxo1* mutant allele in which exons 2 and 3 are flanked by *lox* sites. The structures of the genomic locus, the targeting vector, and the targeted allele are shown. *FRT-Neo-FRT*, neomycin resistance cassette flanked by *FRT* sites. TK1, thymidine kinase. **b**, Table of viable off-spring from *Tie2-cre;Foxo1*$^{flox/+}$ (male) and *Foxo1*$^{flox/flox}$ (female) intercrosses. **c**, Control (*Foxo1*$^{flox/flox}$) and *Foxo1*$^{EC-KO}$ mutants

(*Tie2-cre;Foxo1*^{floxflox}) at E10.5. **d**, PCR of genomic DNA from P5 control (*Foxo1*$^{flox/flox}$ – lane 1 and 3) and *Foxo1*$^{iEC\text{-}KO}$ (*Pdgfb-CreERT;Foxo1*$^{flox/flox}$ – lane 2 and 4) pups untreated (lane 1 and 2) or treated (lane 3 and 4) with 4-OHT. Recombination of the floxed *Foxo1* allele (Δ) occurs only in 4OHT-injected animals that are *Pdgfb-CreERT2*-positive. **e**, Immunofluorescence staining for FOXO1 , VE-cadherin (VECAD) and isolectin-B4 (IB4) in a P5 mouse retina of 4OHT-injected control and *Foxo1*$^{iEC\text{-}KO}$ mice. **f**, Confocal images of *mTmG*$^{+}$ control- and *Foxo1*$^{iEC\text{-}KO}$ mice that were injected with 4-OHT from P1 – P4 and analysed for GFP, ERG and IB4 expression.

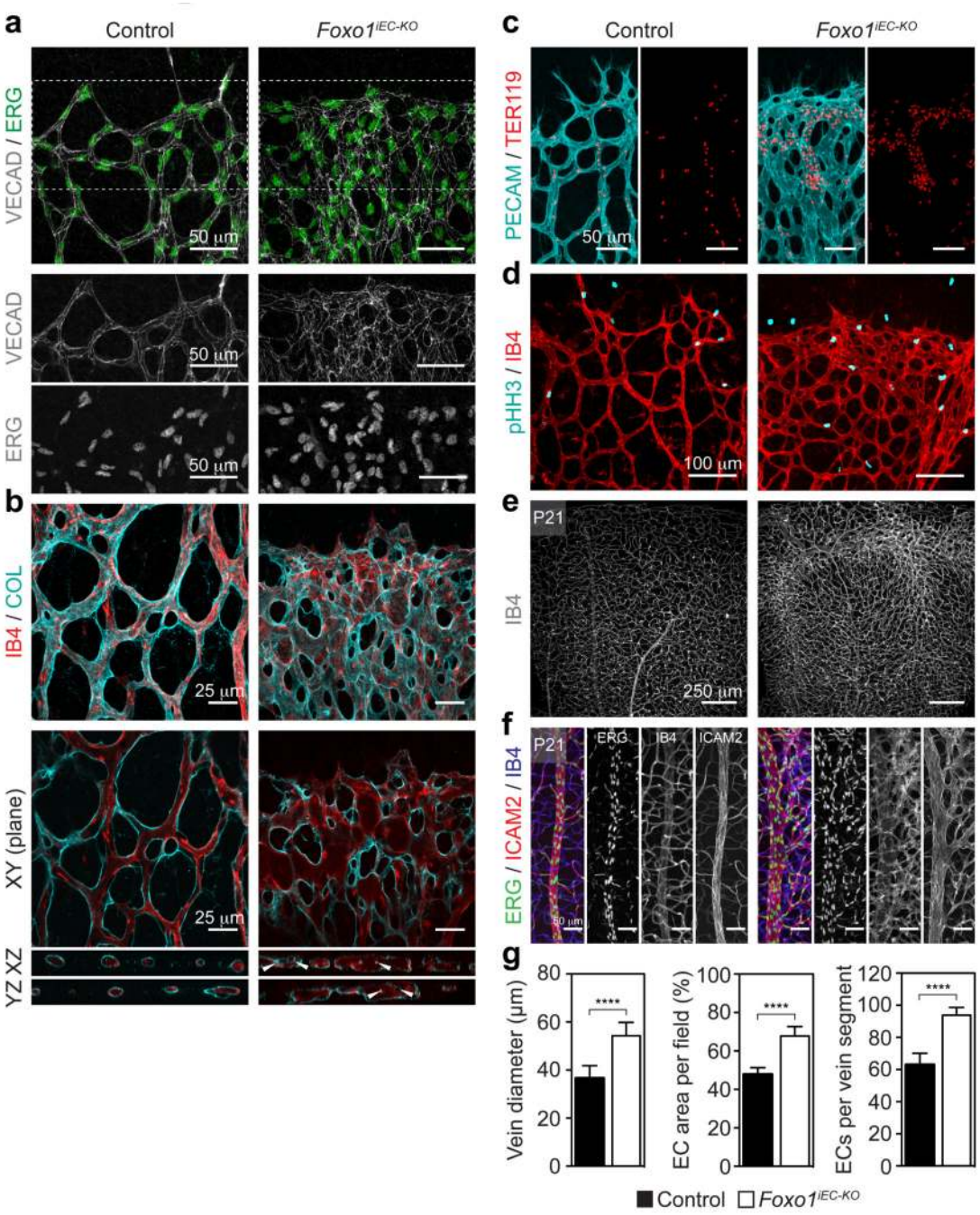

Extended Data Figure 2. Endothelial FOXO1 deficiency leads to abnormal vessel size and shape

a, Immunostaining for VECAD and ERG in *Foxo1*$^{iEC\text{-}KO}$ and control retinas. The lower panels show the isolated VECAD and ERG signals of the inset. **b**, Confocal images showing maximum intensity projections and XY, XZ, and YZ planes of a thick stack of IB4 and collagen IV (COL) stained P5 retinas. *Foxo1*$^{iEC\text{-}KO}$ mice develop enlarged vessels with abnormal lumen organisation. White arrowheads point to areas with multiple vessel layers and intraluminal collagen strands. **c**, Images of IB4 (cyan) and TER119 (red) stained P5 retinas of control and *Foxo1*$^{iEC\text{-}KO}$ mice. Note that aggregates of TER119^{+} red blood cells

Europe PMC Funders Author Manuscripts

form in *Foxo1*$^{iEC\text{-}KO}$ but not in control mice. **d**, Phospho-histone H3 (pHH3) and IB4 immunostaining of P5 *Foxo1*$^{iEC\text{-}KO}$ and control mice. **e**, Images of IB4 stained retinas at P21 showing an increased vessel density in *Foxo1*$^{iEC\text{-}KO}$ mice (same samples as in Figure 1h). **f**, Higher magnification images of ERG , ICAM2 and IB4 stained retinas at P21 showing increased numbers of ECs in the perivenous plexus of *Foxo1*$^{iEC\text{-}KO}$ mice. **g**, Bar graphs showing the mean endothelial area (n ≥8), mean diameter of central vein (n ≥8), and number of ERG/IB4+ cells (n ≥4) in P21 retinas of *Foxo1*$^{iEC\text{-}KO}$ and control mice. Data represent mean ± s.d. Two-tailed unpaired *t*-test. ****$P < 0.0001$.

Europe PMC Funders Author Manuscripts

Europe PMC Funders Author Manuscripts

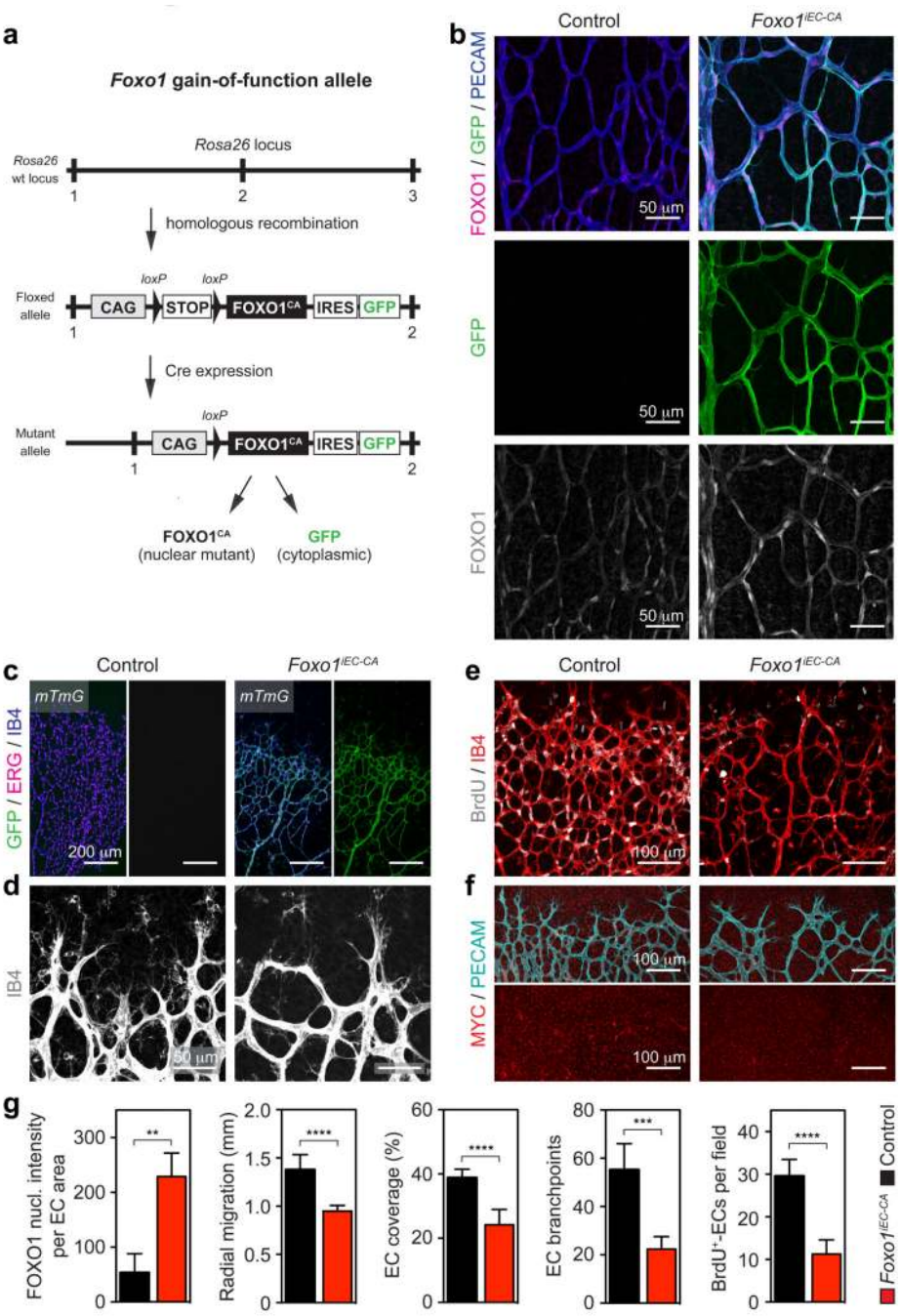

Extended Data Figure 3. Inducible overexpression of a constitutively active FOXO1 mutant in ECs of mice

a, A cassette containing the *CAG* promoter, a floxed *STOP* sequence, a cDNA encoding for *Foxo1*^{CA}, and *IRES-GFP* was inserted into the *Rosa26* locus. A schematic representation of the wild-type *Rosa26 locus*, the floxed allele, and the recombined allele following *Cre* expression is shown. **b**, Immunofluorescence staining for FOXO1 , GFP and PECAM in P5 *Foxo1*$^{iEC-CA}$ and control mice. **c**, Confocal images of *mTmG*$^{+}$ control- and *Foxo1*$^{iEC-CA}$ mice that were injected with 4-OHT from P1 – P4 and analysed for GFP, ERG and IB4

Europe PMC Funders Author Manuscripts

expression. The right half of both images shows the GFP signal alone. **d**, High-magnification images of iB4-stained retinal vessels at the angiogenic front in control and *Foxo1*$^{iEC\text{-}CA}$ pups. **e**, BrdU and IB4 labelling of whole-mount P5 retinas reveals reduced endothelial proliferation in *Foxo1*$^{iEC\text{-}CA}$ animals. **f**, Confocal images showing MYC and PECAM immunostaining in P5 retinas of control and *Foxo1*$^{iEC\text{-}CA}$ mice. The lower half of both images shows the MYC signal alone. **g**, Quantification of FOXO1 nuclear staining intensity in ECs (n = 3), radial migration (n = 10), endothelial coverage (n = 10), branch points (n = 10), and endothelial BrdU incorporation (n ≥6) in P5 retinas of control and *Foxo1*$^{iEC\text{-}CA}$ mutant mice. Data represent mean ± s.d. Two-tailed unpaired *t*-test. $^{**}P < 0.01$; $^{***}P < 0.001$; $^{****}P < 0.0001$.

Europe PMC Funders Author Manuscripts

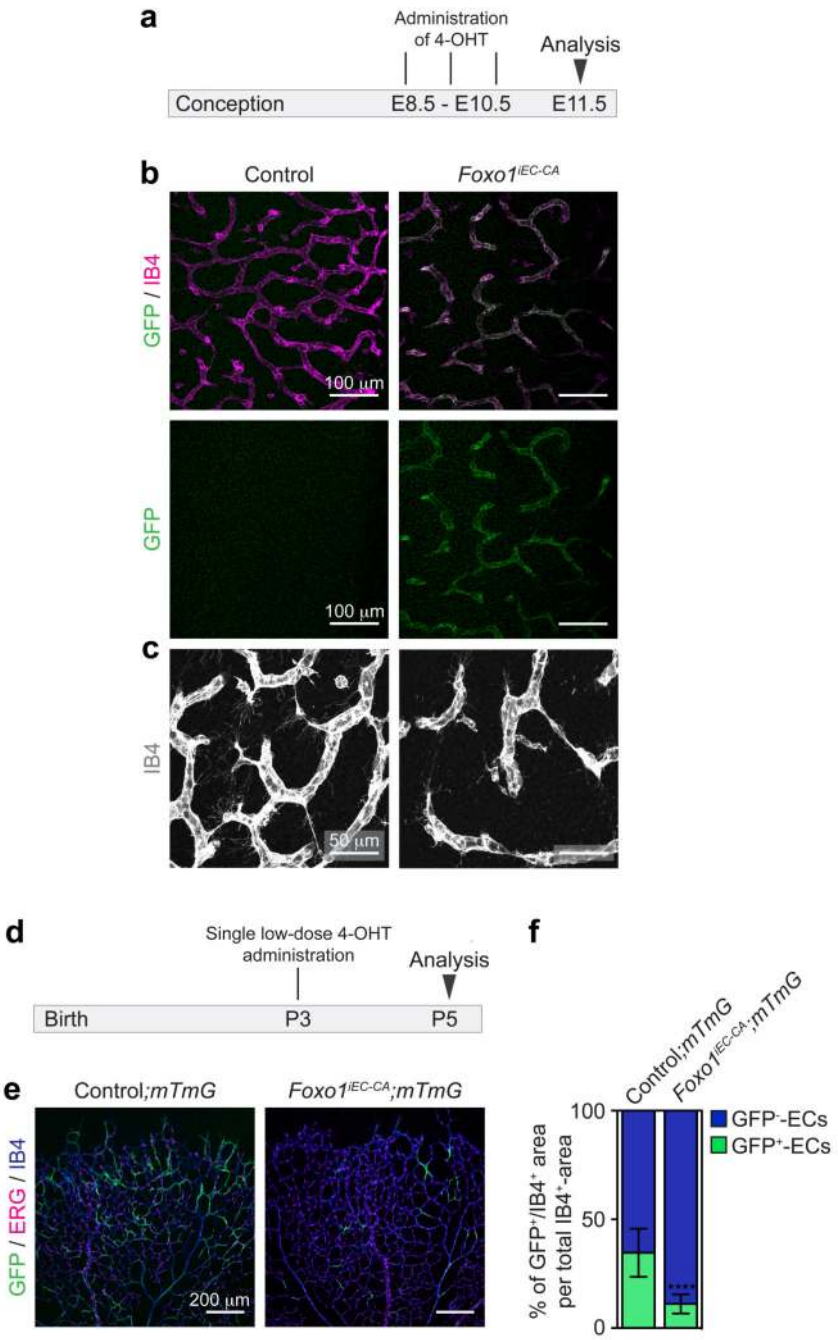

Extended Data Figure 4. FOXO1 restricts EC propagation and vascular growth in a cell-autonomous manner

a, Timeline for the analysis of angiogenesis in the embryonic hindbrain. Plug-positive female mice were injected with 4OHT from embryonic day (E) 8.5 to 10.5 and embryos harvested on E11.5 for hindbrain dissection. **b**, Confocal images of E11.5 control and *Foxo1*$^{iEC\text{-}CA}$ hindbrains stained with IB4 and GFP. **c**, High-magnification images of IB4-stained blood vessels in the ventricular zone of control and *Foxo1*$^{iEC\text{-}CA}$ mice. **d**, Timeline for the analysis of control and *Foxo1*$^{iEC\text{-}CA}$ low-degree chimeras that heterozygously co-

express the *mTmG* Cre reporter. Control and *Foxo1*$^{iEC\text{-}KO}$ mice were injected with a single low-dose of 4OHT at P3 and retinas analysed at P5. **e**,**f**, Confocal images (e) and quantification (f) of control;*mTmG* and *Foxo1*^{iECCA};*mTmG* retinas after low-dose 4-OHT treatment at P3 (n = 9). Samples were labelled for GFP, ERG and IB4. Data represent mean ± s.d., two-tailed unpaired *t*-test. ****$P < 0.0001$.

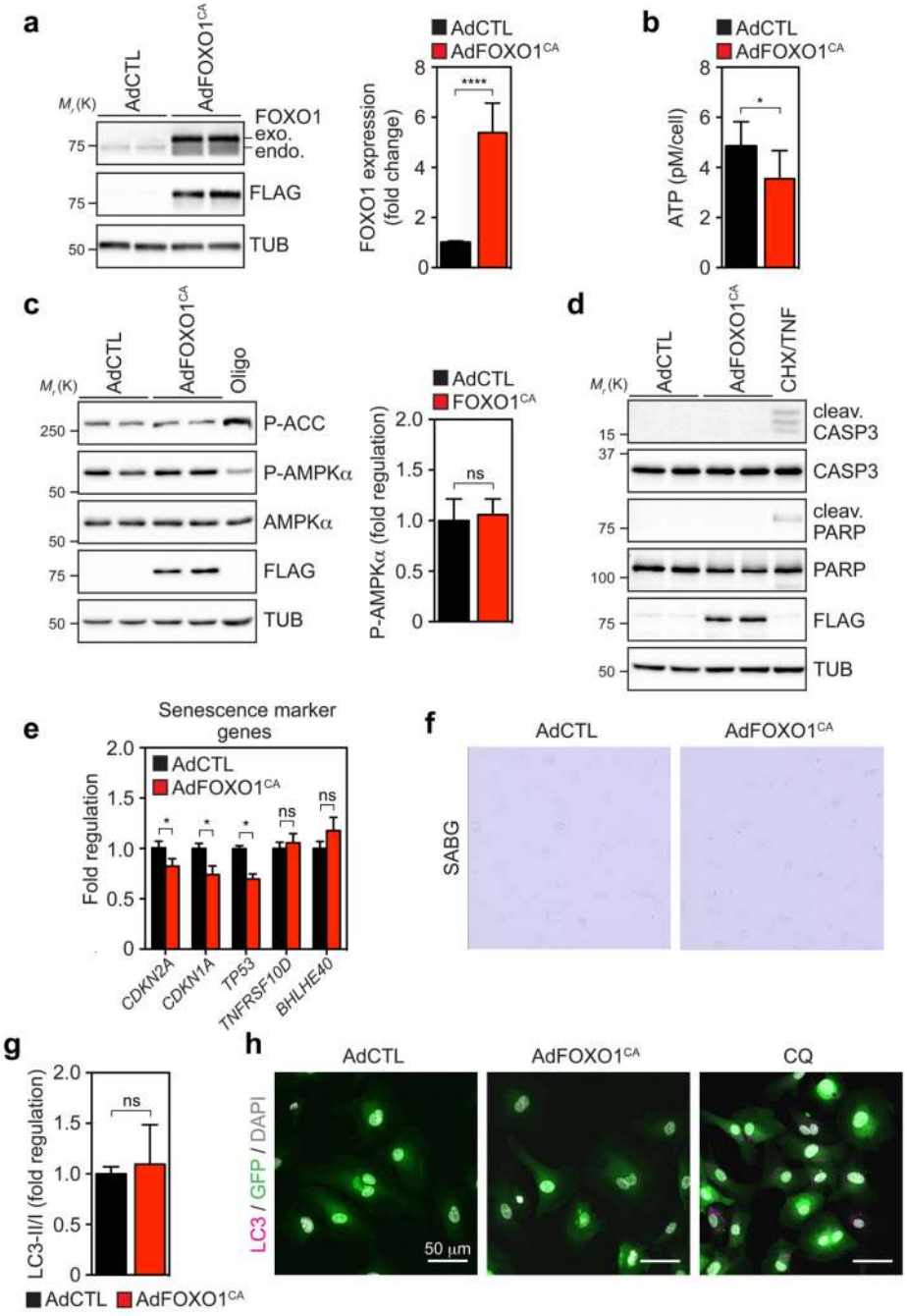

Extended Data Figure 5. Forced expression of FOXO1 does not induce apoptosis, senescence, autophagy or energy distress in cultured ECs

Europe PMC Funders Author Manuscripts

Europe PMC Funders Author Manuscripts

a, Immunoblot analysis and quantification of FOXO1 protein levels in AdCTL and AdFOXO1^{CA}-Flag transduced HUVEC (n = 20). **b**, ATP levels in ECs 24 hours post transduction with AdCTL or AdFOXO1^{CA} (n = 7). **c**, Western blot images and quantification of AdCTL- or AdFOXO1^{CA}-Flag-transduced HUVEC showing that FOXO1^{CA} does not alter the phosphorylation of AMPKα (Thr^{172}) or of its substrate ACC (Ser^{79}). Oligomycin (Oligo), positive control. TUB, Tubulin. (n = 10). **d**, Western blotting of AdCTL- or AdFOXO1^{CA}-Flag-transduced HUVEC illustrating that overexpression of FOXO1^{CA} does not induce apoptotic cell death. Cleaved Caspase3 (CASP3) and PARP served as markers of apoptosis. Cycloheximide (CHX) and TNFα (TNF) costimulation, positive control. **e**, Analysis of senescence-associated genes by microarray demonstrating that senescence markers were not significantly changed or even down-regulated in FOXO1^{CA}-overexpressing ECs. (n = 3). **f**, Images of ß-galactosidase stainings in AdCTL and AdFOXO1^{CA}-transduced HUVEC showing no increase in senescence-associated ß-galactosidase activity (SABG). **g**, Densitometric quantification of the LC3-II to LC3-I ratio in AdCTL- or AdFOXO1^{CA} -transduced HUVEC (n = 10). **h**, Immunofluorescence analysis of AdCTL- and AdFOXO1^{CA}-transduced HUVECs (both coexpressing GFP) using LC3 and GFP antibodies. Chloroquine (CQ), positive control. DAPI, endothelial nuclei. Data in a-c, e and g represent mean ± s.d. Two-tailed unpaired *t*-test. *$P < 0.05$; ****$P < 0.0001$; ns, not significant.

Europe PMC Funders Author Manuscripts

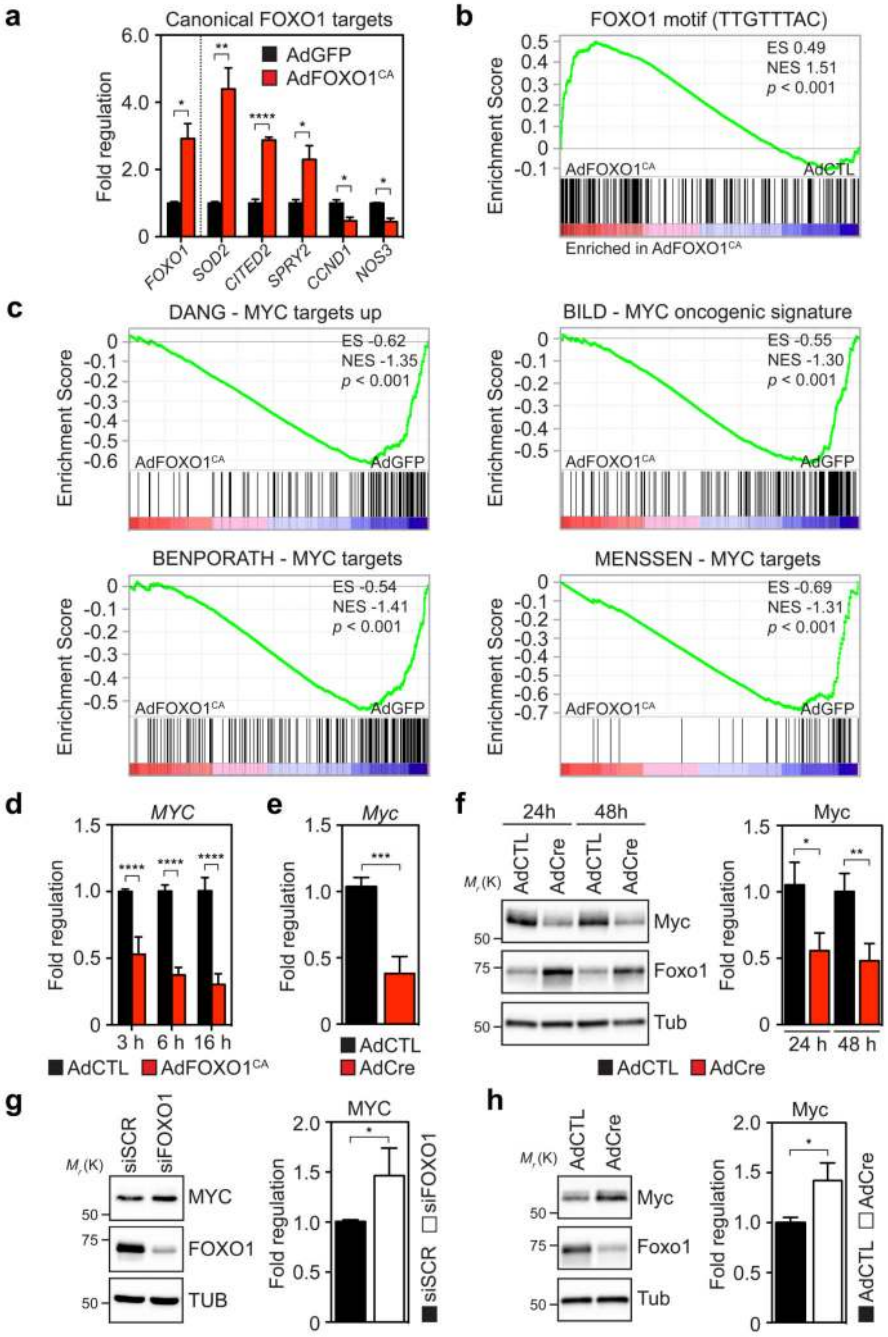

Extended Data Figure 6. FOXO1 represses MYC signalling in ECs

a, Microarray expression analysis of FOXO1 and of canonical FOXO target genes in AdFOXO1^{CA}- and AdCTL-expressing HUVECs 16 hours post transduction (n = 3). **b**, GSEA of the FOXO1 DNA binding element (TTGTTTAC) gene set in AdFOXO1^{CA}- or AdCTL-transduced ECs. ES, enrichment score, NES, normalized enrichment score. **c**, GSEA of MYC gene signatures[39-42] showing the downregulation of MYC target genes in FOXO1^{CA}-expressing HUVECs. **d**, qPCR expression analysis of *MYC* at 3, 6 and 16 hours in AdCTL and AdFOXO1^{CA}-transduced HUVECs (n ≥4). **e**, qPCR analysis (n = 4) of *Myc*

Europe PMC Funders Author Manuscripts

mRNA levels in ECs isolated from Foxo1^{CA} mice 24 hours post transduction with a control- or Cre (AdCre) adenovirus. **f**, Immunoblot analysis of Myc in ECs isolated from *Foxo1*^{CA} mice following transduction with AdCTL or AdCre (n = 3). Cre-mediated recombination gave rise to a 2.8 ± 0.3–fold increase in Foxo1 protein expression. **g**, Expression analysis of MYC in HUVECs by Western blotting following RNAi-mediated knockdown of FOXO1 (siFOXO1). siSCR, scrambled control (n = 3). **h**, Myc protein expression in ECs isolated from *Foxo1*^{flox} mice 24 hours post transduction with a AdCTL or AdCre-encoding adenovirus (n = 3). Data in a and d-h represent mean ± s.d., two-tailed unpaired *t*-test. . **P* < 0.05; ***P* < 0.01; ****P* < 0.001; *****P* < 0.0001.

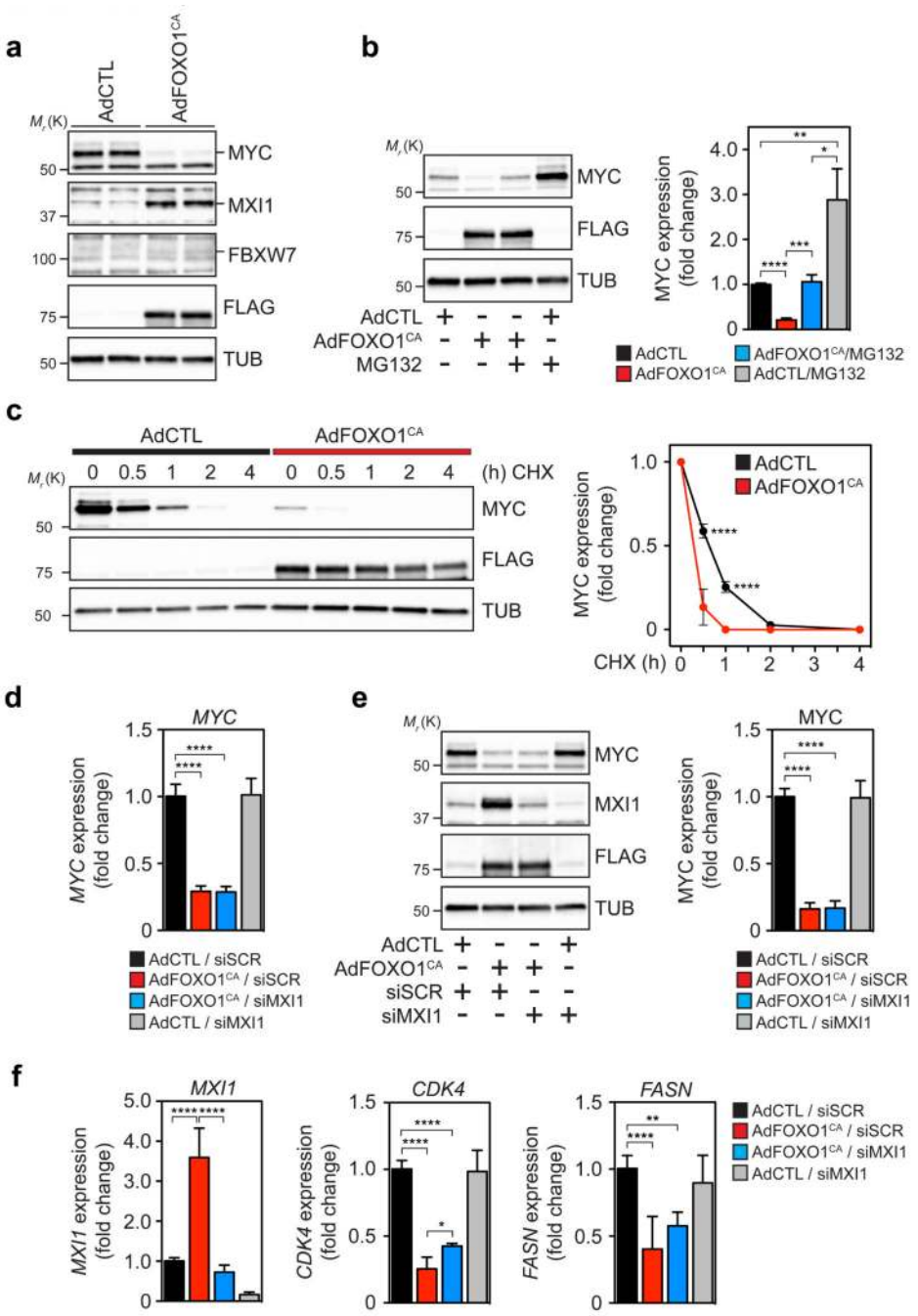

Extended Data Figure 7. FOXO1 interferes with MYC signalling at different levels

a, Western blot analysis of MYC, MXI1 and FBXW7 in AdCTL- or AdFOXO1^{CA}-Flag-transduced HUVEC. **b**, Immunoblot analysis and quantification of MYC protein levels in AdCTL and AdFOXO1^{CA}-Flag transduced HUVECs that were co-treated with the proteasomal inhibitor MG132 (n = 3). **c**, Analysis of MYC protein half-life in AdCTL- or AdFOXO1CA-Flag-transduced HUVECs. The day after transduction, HUVECs were treated with cylcoheximide (CHX) and incubated for the times indicated (h, hours). Data represent mean ± s.d. Two-way ANOVA with Bonferroni's multiple comparison post-hoc test. **d**,**e**,

qPCR (d) and immunoblot analysis (e) of MYC levels in control (siSCR) or MXI1 (siMXI1) siRNA-transfected HUVECs that were also transduced with AdCTL or AdFOXO1^{CA}-Flag (n ≥5). **f**, qPCR analysis of MYC target genes in siSCR or siMXI1-transfected HUVECs that were cotransduced with AdCTL or AdFOXO1^{CA} (n ≥3).. Data represent mean ± s.d. One-way ANOVA with Bonferroni's multiple comparison post-hoc test was performed in b, d, e and f. $^{**}P < 0.01$; $^{***}P < 0.001$; $^{****}P < 0.0001$.

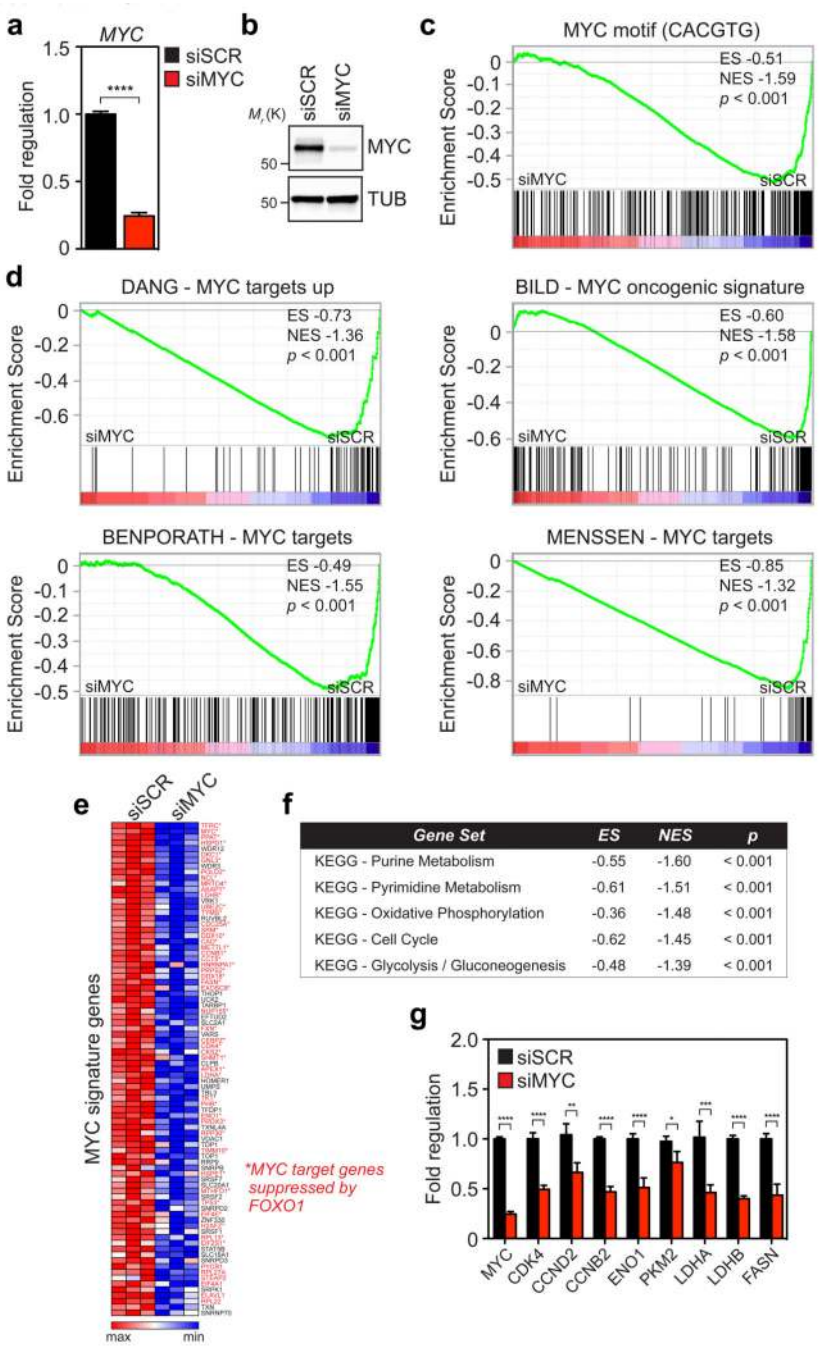

Extended Data Figure 8. MYC regulates genes involved in endothelial metabolism and growth in ECs

Europe PMC Funders Author Manuscripts

Europe PMC Funders Author Manuscripts

a,**b**, Analysis of MYC expression by qPCR (a) and immunoblot (b) in scrambled (siSCR) and MYC (siMYC) siRNA-treated HUVECs 24 h post transfection (n = 7). **c**, GSEA of the MYC-(CACGTG) DNA binding element gene set in siSCR or siMYC-transfected HUVECs. **d**, GSEA of MYC gene signatures[39-42] showing the downregulation of MYC target genes in MYC-depleted HUVECs. **e**, Heatmap of downregulated MYC signature genes in MYC-silenced HUVECs (n = 3). Genes highlighted in red indicate genes that are also suppressed by $FOXO1^{CA}$ overexpression. **f**, Table of KEGG gene sets enriched among genes downregulated in the MYC siRNA-transfected ECs. **g**, Expression analysis of FOXO1-regulated MYC target genes by qPCR in MYC-silenced HUVECs (n ≥4). Data in a and g represent mean ± s.d., two-tailed unpaired *t*-test. $*P < 0.05$; $**P < 0.01$; $***P < 0.001$; $****P < 0.0001$.

Europe PMC Funders Author Manuscripts

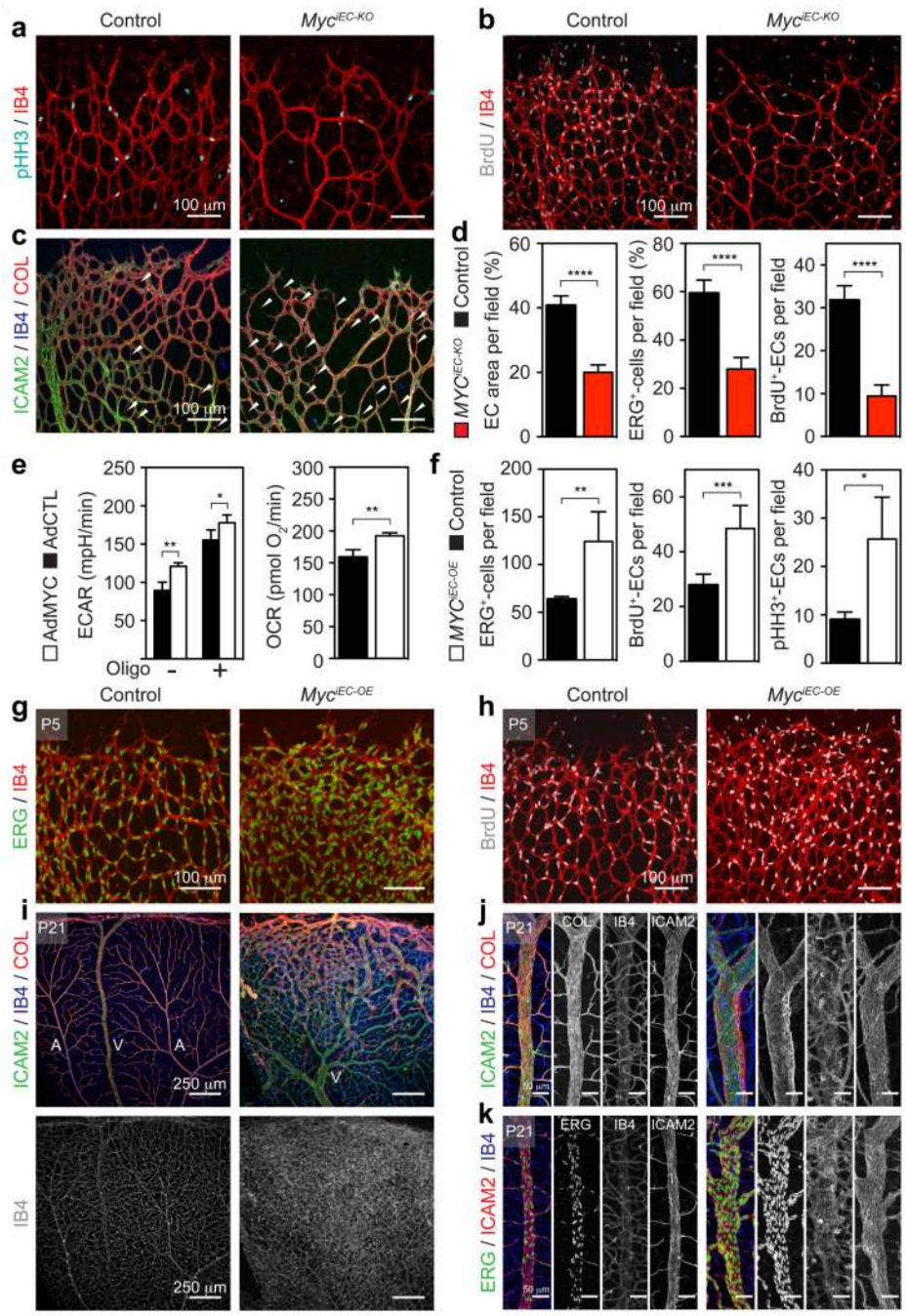

Extended Data Figure 9. MYC is a critical driver of endothelial proliferation, growth and metabolism

a,**b**, IB4 and pHH3 (a) or BrdU (b) labelling of P5 retinas reveals reduced endothelial proliferation in *Myc*$^{iEC\text{-}KO}$ mice. **c**, ICAM2, IB4 and COL staining of retinas at P5 showing an increased number of empty (COL^{+}, IB4^{-}-negative) sleeves (white arrows) in the plexus of *Myc*$^{iEC\text{-}KO}$ mutants. **d**, Quantitative analysis of the indicated vascular parameters in P5 retinas of control and *Myc*$^{iEC\text{-}KO}$ mice (n ≥8). **e**, ECAR (n = 4) and OCR (n = 4) in AdMYC-transduced HUVECs showing a heightened metabolic activity in MYC-

overexpressing ECs (6.8 ± 1.4-fold MYC overexpression). **f**, *Pdgfb-creERT2*-mediated overexpression of Myc (2.4 ± 0.8-fold Myc overexpression) enhances vascular growth as indicated by the parameters assessed at P5 (n ≥6). **g**, ERG and IB4 labelling of P5 retinas showing an increase in cellularity in vessels of $Myc^{iEC\text{-}OE}$ mice. **h**, Enhanced EC proliferation in $Myc^{iEC\text{-}OE}$ mice as revealed by BrdU and IB4 costaining. **i**,**j**, Overview (i) and higher magnification images (j) of ICAM2, IB4 and COL stained retinas at P21 showing aberrant vascular growth and venous enlargement in $Myc^{iEC\text{-}OE}$ mice. **k**, Increased endothelial cellularity in veins of $Myc^{iEC\text{-}OE}$ mice at P21. Data in d-f represent mean ± s.d., two-tailed unpaired *t*-test. $^{*}P < 0.05$; $^{**}P < 0.01$; $^{***}P < 0.001$; $^{****}P < 0.0001$.

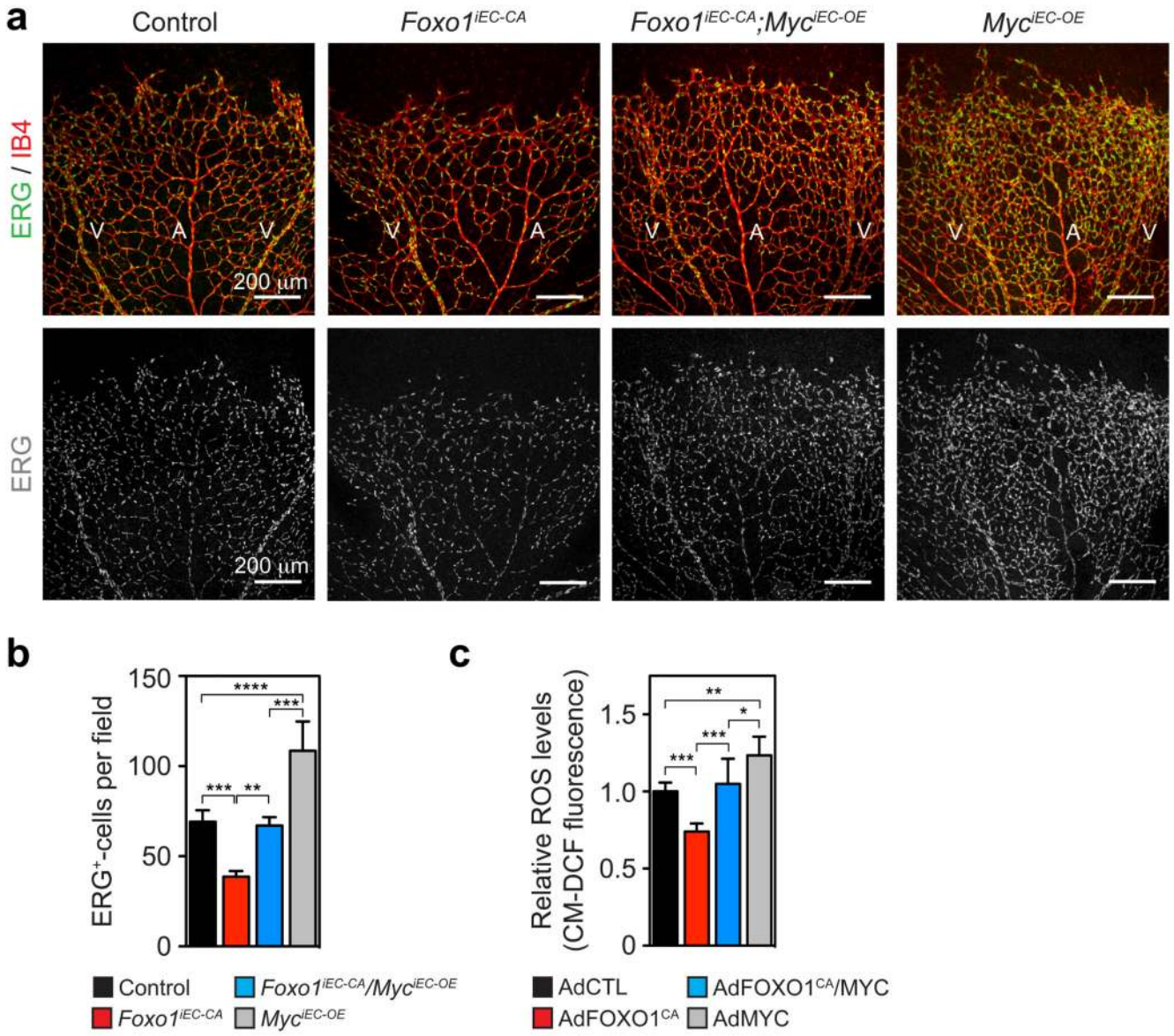

Extended Data Figure 10. Restoration of MYC signalling in FOXO1^{CA}-overexpressing endothelium restores vascular growth

Europe PMC Funders Author Manuscripts

a,**b**, Confocal images (a) and quantification (b) of ERG and IB4 stained P5 retinas in control, *Foxo1*$^{iEC\text{-}CA}$, *Myc*$^{iEC\text{-}OE}$ and *Foxo1*$^{iEC\text{-}CA}$/*Myc*$^{iEC\text{-}OE}$ mice (same samples as in Figure 4h) showing that EC numbers are normalized in the *Foxo1*$^{iEC\text{-}CA}$/*Myc*$^{iEC\text{-}OE}$ double mutants (n ≥3). **c**, Relative ROS levels in AdCTL, AdFOXO1^{CA}, AdFOXO1^{CA}/AdMYC and AdMYC-transduced HUVECs showing that ROS levels increase again in FOXO1^{CA}/MYC co-expressing ECs (n ≥6). Data in b and c represent mean ± s.d., one-way ANOVA with Bonferroni's multiple comparison post-hoc test. *$P < 0.05$; **$P < 0.01$; ***$P < 0.001$; ****$P < 0.0001$.

Supplementary Material

Refer to Web version on PubMed Central for supplementary material.

Acknowledgements

We thank Frederick W. Alt and Ioannis Aifantis for *Myc*^{flox} mice, and Tanja Enders, Julia Sperling, and Kevin Wilson for assistance with the mouse colony. The research of M.P. is supported by the Max Planck Society, a European Research Council Starting Grant (ANGIOMET), the Deutsche Forschungsgemeinschaft (SFB 834), the Excellence Cluster Cardiopulmonary System (EXC 147/1), the Cluster of Excellence Macromolecular Complexes (EXC115), the Foundation Leducq Transatlantic Network (ARTEMIS), the German Center for Cardiovascular Research DZHK (BMBF), the LOEWE grant Ub-Net, and the European Molecular Biology Organization Young Investigator Programme. The research of K.R. is supported by an ERC Advanced Grant (268921). I.M.A. is a recipient of a DOC-fFORTE fellowship of the Austrian Academy of Sciences.

References

1. Ghesquiere B, Wong BW, Kuchnio A, Carmeliet P. Metabolism of stromal and immune cells in health and disease. Nature. 2014; 511:167–176. [PubMed: 25008522]
2. Adams RH, Alitalo K. Molecular regulation of angiogenesis and lymphangiogenesis. Nat Rev Mol Cell Biol. 2007; 8:464–478. [PubMed: 17522591]
3. Potente M, Gerhardt H, Carmeliet P. Basic and therapeutic aspects of angiogenesis. Cell. 2011; 146:873–887. [PubMed: 21925313]
4. De Bock K, Georgiadou M, Carmeliet P. Role of endothelial cell metabolism in vessel sprouting. Cell Metabolism. 2013; 18:634–647. [PubMed: 23973331]
5. Dang CV. MYC, metabolism, cell growth, and tumorigenesis. Cold Spring Harb Perspect Med. 2013; 3
6. Adhikary S, Eilers M. Transcriptional regulation and transformation by Myc proteins. Nat Rev Mol Cell Biol. 2005; 6:635–645. [PubMed: 16064138]
7. Vander Heiden MG, Cantley LC, Thompson CB. Understanding the Warburg effect: the metabolic requirements of cell proliferation. Science. 2009; 324:1029–1033. [PubMed: 19460998]
8. Ward PS, Thompson CB. Metabolic reprogramming: a cancer hallmark even warburg did not anticipate. Cancer Cell. 2012; 21:297–308. [PubMed: 22439925]
9. Salih DA, Brunet A. FoxO transcription factors in the maintenance of cellular homeostasis during aging. Curr Opin Cell Biol. 2008; 20:126–136. [PubMed: 18394876]
10. Eijkelenboom A, Burgering BM. FOXOs: signalling integrators for homeostasis maintenance. Nat Rev Mol Cell Biol. 2013; 14:83–97. [PubMed: 23325358]
11. Daly C, et al. Angiopoietin-1 modulates endothelial cell function and gene expression via the transcription factor FKHR (FOXO1). Genes Dev. 2004; 18:1060–1071. [PubMed: 15132996]
12. Potente M, et al. Involvement of Foxo transcription factors in angiogenesis and postnatal neovascularization. J Clin Invest. 2005; 115:2382–2392. [PubMed: 16100571]
13. Paik JH, et al. FoxOs are lineage-restricted redundant tumor suppressors and regulate endothelial cell homeostasis. Cell. 2007; 128:309–323. [PubMed: 17254969]

14. Taddei A, et al. Endothelial adherens junctions control tight junctions by VE-cadherin-mediated upregulation of claudin-5. Nature Cell Biology. 2008; 10:923–934. [PubMed: 18604199]
15. Tsuchiya K, et al. FoxOs integrate pleiotropic actions of insulin in vascular endothelium to protect mice from atherosclerosis. Cell Metabolism. 2012; 15:372–381. [PubMed: 22405072]
16. Keller C, et al. Alveolar rhabdomyosarcomas in conditional Pax3:Fkhr mice: cooperativity of Ink4a/ARF and Trp53 loss of function. Genes Dev. 2004; 18:2614–2626. [PubMed: 15489287]
17. Sengupta A, Chakraborty S, Paik J, Yutzey KE, Evans-Anderson HJ. FoxO1 is required in endothelial but not myocardial cell lineages during cardiovascular development. Dev Dyn. 2012; 241:803–813. [PubMed: 22411556]
18. Stohr O, et al. Insulin receptor signaling mediates APP processing and beta-amyloid accumulation without altering survival in a transgenic mouse model of Alzheimer's disease. Age. 2013; 35:83–101. [PubMed: 22057897]
19. Delpuech O, et al. Induction of Mxi1-SR alpha by FOXO3a contributes to repression of Myc-dependent gene expression. Mol Cell Biol. 2007; 27:4917–4930. [PubMed: 17452451]
20. Gan B, et al. FoxOs enforce a progression checkpoint to constrain mTORC1-activated renal tumorigenesis. Cancer Cell. 2010; 18:472–484. [PubMed: 21075312]
21. Jensen KS, et al. FoxO3A promotes metabolic adaptation to hypoxia by antagonizing Myc function. The EMBO journal. 2011; 30:4554–4570. [PubMed: 21915097]
22. Kress TR, et al. The MK5/PRAK kinase and Myc form a negative feedback loop that is disrupted during colorectal tumorigenesis. Mol Cell. 2011; 41:445–457. [PubMed: 21329882]
23. Ferber EC, et al. FOXO3a regulates reactive oxygen metabolism by inhibiting mitochondrial gene expression. Cell Death and Differentiation. 2012; 19:968–979. [PubMed: 22139133]
24. de Alboran IM, et al. Analysis of C-MYC function in normal cells via conditional gene-targeted mutation. Immunity. 2001; 14:45–55. [PubMed: 11163229]
25. Sander S, et al. Synergy between PI3K signaling and MYC in Burkitt lymphomagenesis. Cancer Cell. 2012; 22:167–179. [PubMed: 22897848]
26. Kops GJ, et al. Forkhead transcription factor FOXO3a protects quiescent cells from oxidative stress. Nature. 2002; 419:316–321. [PubMed: 12239572]
27. Nemoto S, Finkel T. Redox regulation of forkhead proteins through a p66shc-dependent signaling pathway. Science. 2002; 295:2450–2452. [PubMed: 11884717]
28. Tothova Z, et al. FoxOs are critical mediators of hematopoietic stem cell resistance to physiologic oxidative stress. Cell. 2007; 128:325–339. [PubMed: 17254970]
29. Miyamoto K, et al. Foxo3a is essential for maintenance of the hematopoietic stem cell pool. Cell Stem Cell. 2007; 1:101–112. [PubMed: 18371339]
30. Yeo H, et al. FoxO3 coordinates metabolic pathways to maintain redox balance in neural stem cells. The EMBO journal. 2013; 32:2589–2602. [PubMed: 24013118]
31. Koni PA, et al. Conditional vascular cell adhesion molecule 1 deletion in mice: impaired lymphocyte migration to bone marrow. The Journal of Experimental Medicine. 2001; 193:741–754. [PubMed: 11257140]
32. Claxton S, et al. Efficient, inducible Cre-recombinase activation in vascular endothelium. Genesis. 2008; 46:74–80. [PubMed: 18257043]
33. Muzumdar MD, Tasic B, Miyamichi K, Li L, Luo L. A global double-fluorescent Cre reporter mouse. Genesis. 2007; 45:593–605. [PubMed: 17868096]
34. Fantin A, Vieira JM, Plein A, Maden CH, Ruhrberg C. The embryonic mouse hindbrain as a qualitative and quantitative model for studying the molecular and cellular mechanisms of angiogenesis. Nat Protoc. 2013; 8:418–429. [PubMed: 23424750]
35. Pitulescu ME, Schmidt I, Benedito R, Adams RH. Inducible gene targeting in the neonatal vasculature and analysis of retinal angiogenesis in mice. Nat Protoc. 2010; 5:1518–1534. [PubMed: 20725067]
36. Guarani V, et al. Acetylation-dependent regulation of endothelial Notch signalling by the SIRT1 deacetylase. Nature. 2011; 473:234–238. [PubMed: 21499261]

37. Ramaswamy S, Nakamura N, Sansal I, Bergeron L, Sellers WR. A novel mechanism of gene regulation and tumor suppression by the transcription factor FKHR. Cancer Cell. 2002; 2:81–91. [PubMed: 12150827]

38. Hermeking H, et al. Identification of CDK4 as a target of c-MYC. Proceedings of the National Academy of Sciences of the United States of America. 2000; 97:2229–2234. [PubMed: 10688915]

39. Zeller KI, Jegga AG, Aronow BJ, O'Donnell KA, Dang CV. An integrated database of genes responsive to the Myc oncogenic transcription factor: identification of direct genomic targets. Genome Biology. 2003; 4:R69. [PubMed: 14519204]

40. Menssen A, Hermeking H. Characterization of the c-MYC-regulated transcriptome by SAGE: identification and analysis of c-MYC target genes. Proceedings of the National Academy of Sciences of the United States of America. 2002; 99:6274–6279. [PubMed: 11983916]

41. Ben-Porath I, et al. An embryonic stem cell-like gene expression signature in poorly differentiated aggressive human tumors. Nature Genetics. 2008; 40:499–507. [PubMed: 18443585]

42. Bild AH, et al. Oncogenic pathway signatures in human cancers as a guide to targeted therapies. Nature. 2006; 439:353–357. [PubMed: 16273092]

Europe PMC Funders Author Manuscripts

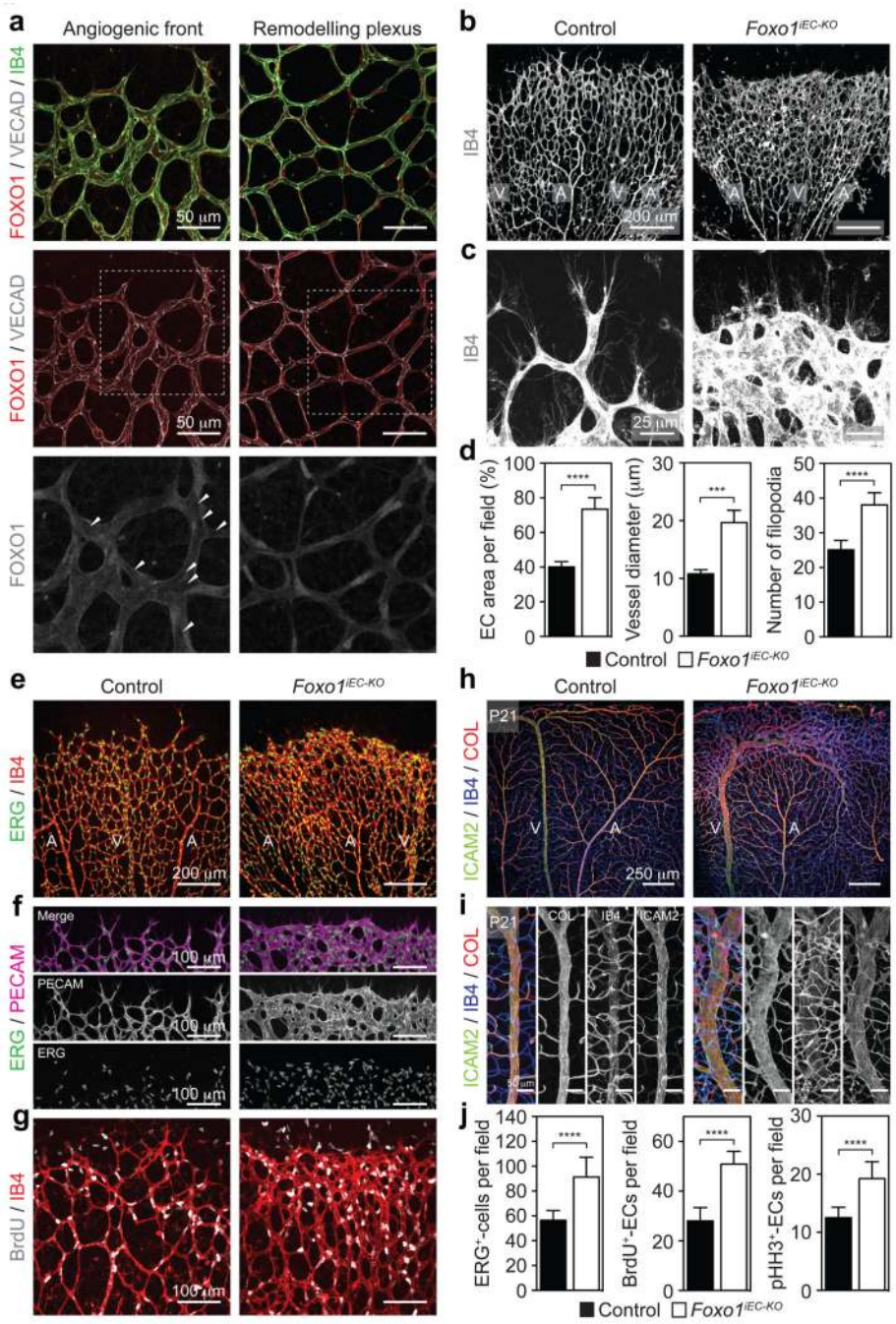

Figure 1. Endothelial FOXO1 is an essential regulator of vascular growth

a, Staining for FOXO1, VE-cadherin (VECAD) and isolectin-B4 (IB4) in a P5 mouse retina. The lower panels depict the FOXO1 signal of the boxed area. Arrowheads point to ECs with weak FOXO1 nuclear staining. **b**,**c**, Overview (b) and higher magnification (c) images of IB4-stained retinal vessels at P5 in *Foxo1*$^{iEC\text{-}KO}$ and controls. A, artery; V, vein. **d**, Bar graphs showing endothelial area (n ≥7), branch diameter (n ≥7), and number of filopodia (n ≥5).**e**, Images of IB4 and ERG stained P5 retinas of control and *Foxo1*$^{iEC\text{-}KO}$ mutants. **f**, PECAM and ERG stained retinas showing endothelial clustering at the angiogenic front in

Foxo1$^{iEC\text{-}KO}$ mutants. **g**, Increased endothelial BrdU incorporation in *Foxo1*$^{iEC\text{-}KO}$ retinas. **h**,**i**, Confocal images of ICAM2 , IB4 and collagen IV (COL) stained retinas at P21. **j**, Quantifications of ERG/IB4- (n ≥9), BrdU/IB4- (n ≥5) and pHH3/IB4- (n ≥7) positive cells. Data in **d** and **j** represent mean ± s.d., two-tailed unpaired *t*-test. ***$P < 0.001$; ****$P < 0.0001$.

Europe PMC Funders Author Manuscripts

Europe PMC Funders Author Manuscripts

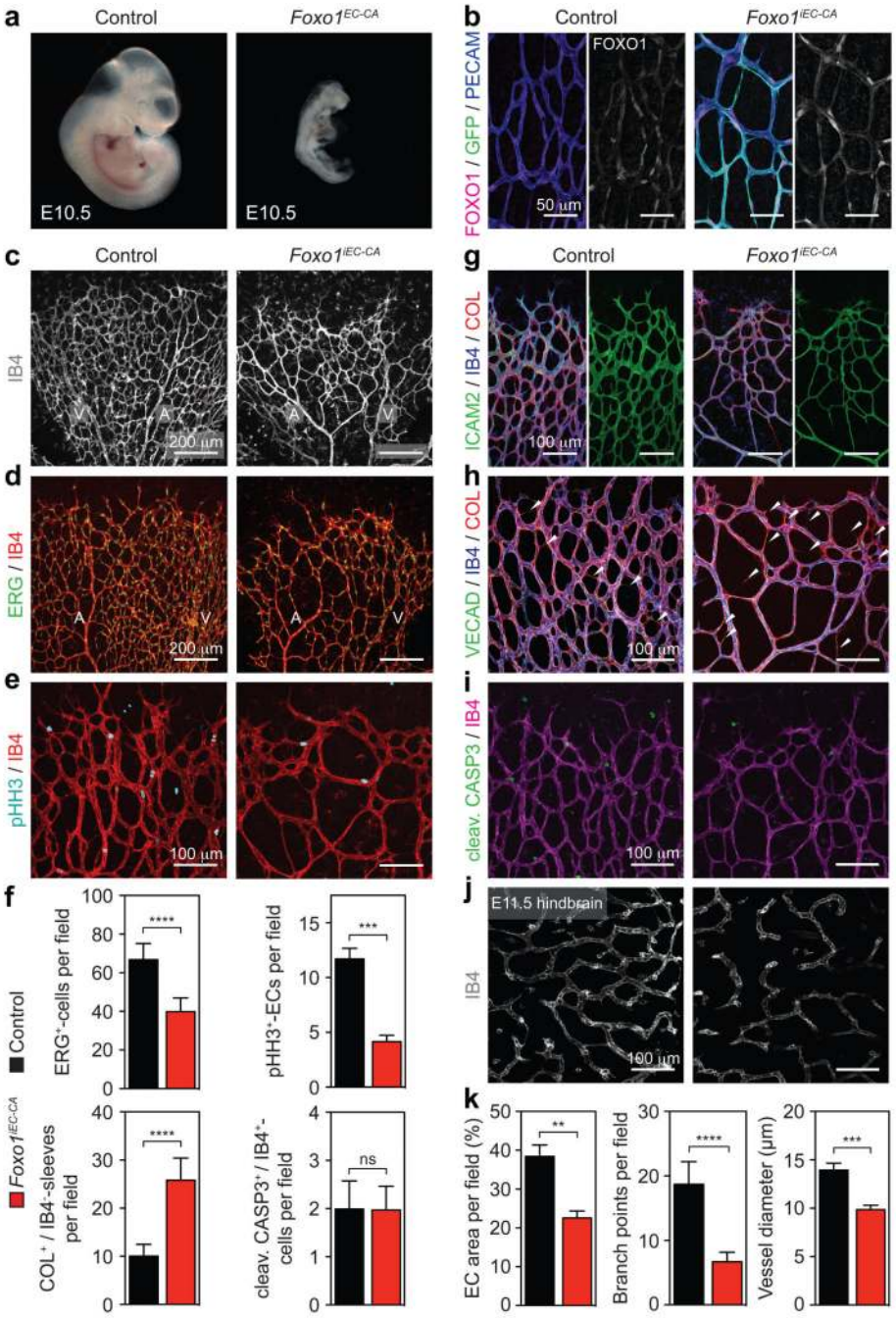

Figure 2. Forced activation of FOXO1 restricts endothelial growth and vascular expansion

a, Overview images of control and *Foxo1*$^{EC\text{-}CA}$ mice at E10.5. **b**, Staining for FOXO1, GFP and PECAM in P5 *Foxo1*$^{iEC\text{-}CA}$ and control mice. **c-e**, IB4- (c), ERG- and IB4- (d), and pHH3- and IB4- (e) labelling of P5 retinas in *Foxo1*$^{iEC\text{-}CA}$ and control mice. **f**, Quantification of vascular parameters in the control and mutant retinas as indicated (n ≥5). **g**, Preserved luminal ICAM2 staining in *Foxo1*$^{iEC\text{-}CA}$ mice. **h**, The number of empty (COL^{+}, IB4^{-}-negative) sleeves (white arrows) in the retinal plexus is increased in the *Foxo1*$^{iEC\text{-}CA}$ mutants. **i**, No difference in cleaved Caspase 3- (CASP3; green) positive ECs between

control and *Foxo1*$^{iEC\text{-}CA}$ mice. **j**, Reduced vascularization of E11.5 hindbrains in *Foxo1*$^{iEC\text{-}CA}$ mice. **k**, Quantification of vascular parameters in control and *Foxo1*$^{iEC\text{-}CA}$ hindbrains (n ≥5). Data in (f) and (k) represent mean ± s.d., two-tailed unpaired *t*-test. $^{**}P < 0.01$; $^{***}P < 0.001$; $^{****}P < 0.0001$.

Europe PMC Funders Author Manuscripts

Europe PMC Funders Author Manuscripts

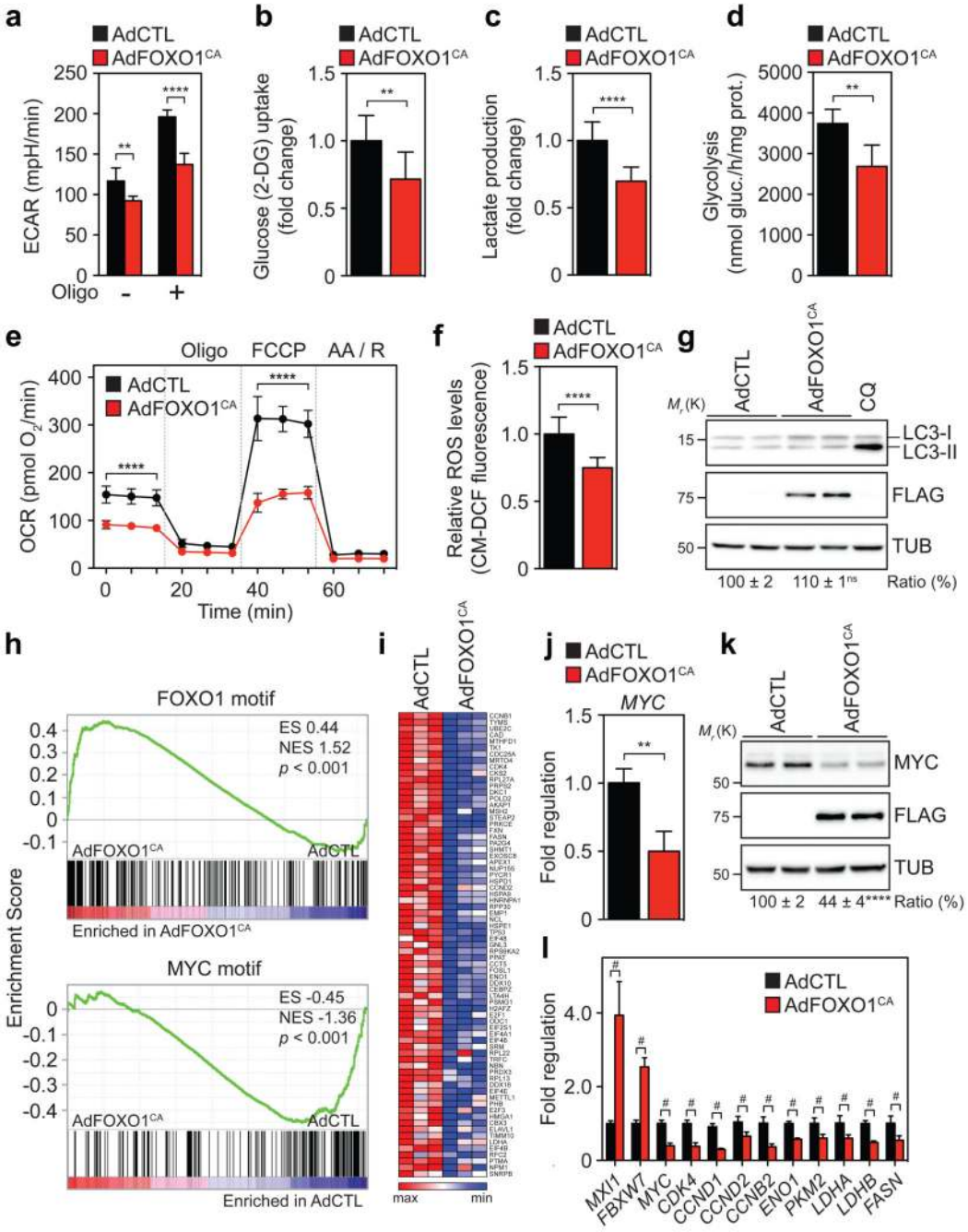

Figure 3. FOXO1 slows endothelial metabolic activity and suppresses MYC signalling

a, Extracellular acidification rate (ECAR) in ECs treated with or without oligomycin (Oligo) showing reduced basal and maximal glycolytic activity in AdFOXO1^{CA}- and AdCTL- (control) transduced HUVECs (n = 6). **b-e**, Reduced 2-deoxy-D-glucose (2-DG) uptake (b; n = 13), relative lactate production (c; n = 10), and glycolytic flux analysis (d; n = 4) in FOXO1^{CA}-expressing ECs **e**, Oxygen consumption rates (OCR) in control and FOXO1^{CA}-overexpressing ECs (n = 5) under basal conditions and in response to oligomycin (Oligo), fluoro-carbonyl cyanide phenylhydrazone (FCCP) or antimycin A (AA) and rotenone (R)..

Europe PMC Funders Author Manuscripts

Data represent mean ± s.d. Two-way ANOVA with Bonferroni's multiple comparison test. **f**, Relative ROS levels in AdCTL- or AdFOXO1^{CA}-transduced ECs (n = 7). **g**, LC3 Western blot analysis showing that overexpression of the Flag-tagged FOXO1^{CA} does not induce autophagy in ECs. CQ, Chloroquine, TUB, Tubulin. Densitometric quantifications are shown below the lanes (n = 10). **h**, GSEA of the FOXO1- (AAACAA) or MYC- (CACGTG) DNA binding element gene sets in AdFOXO1^{CA}- or AdCTL-transduced ECs. ES, enrichment score, NES, normalized enrichment score. **i**, Heatmap of downregulated MYC signature genes in FOXO1^{CA}-overexpressing ECs (n=3). **j,k**, Analysis of MYC expression by microarray (j) and immunoblot (k) in FOXO1^{CA}-Flag-overexpressing endothelium. (j, n = 6; k, n= 10). **l**, Quantitative polymerase chain reaction (qPCR) expression analysis of FOXO1^{CA}-regulated genes involved in MYC signalling(n ≥3). Data in a-d, f, g, j- l represent mean ± s.d., two-tailed unpaired *t*-test. *$P < 0.05$; **$P < 0.01$; ****$P < 0.0001$; $^{\#}P < 00.1$; ns, not significant

Europe PMC Funders Author Manuscripts

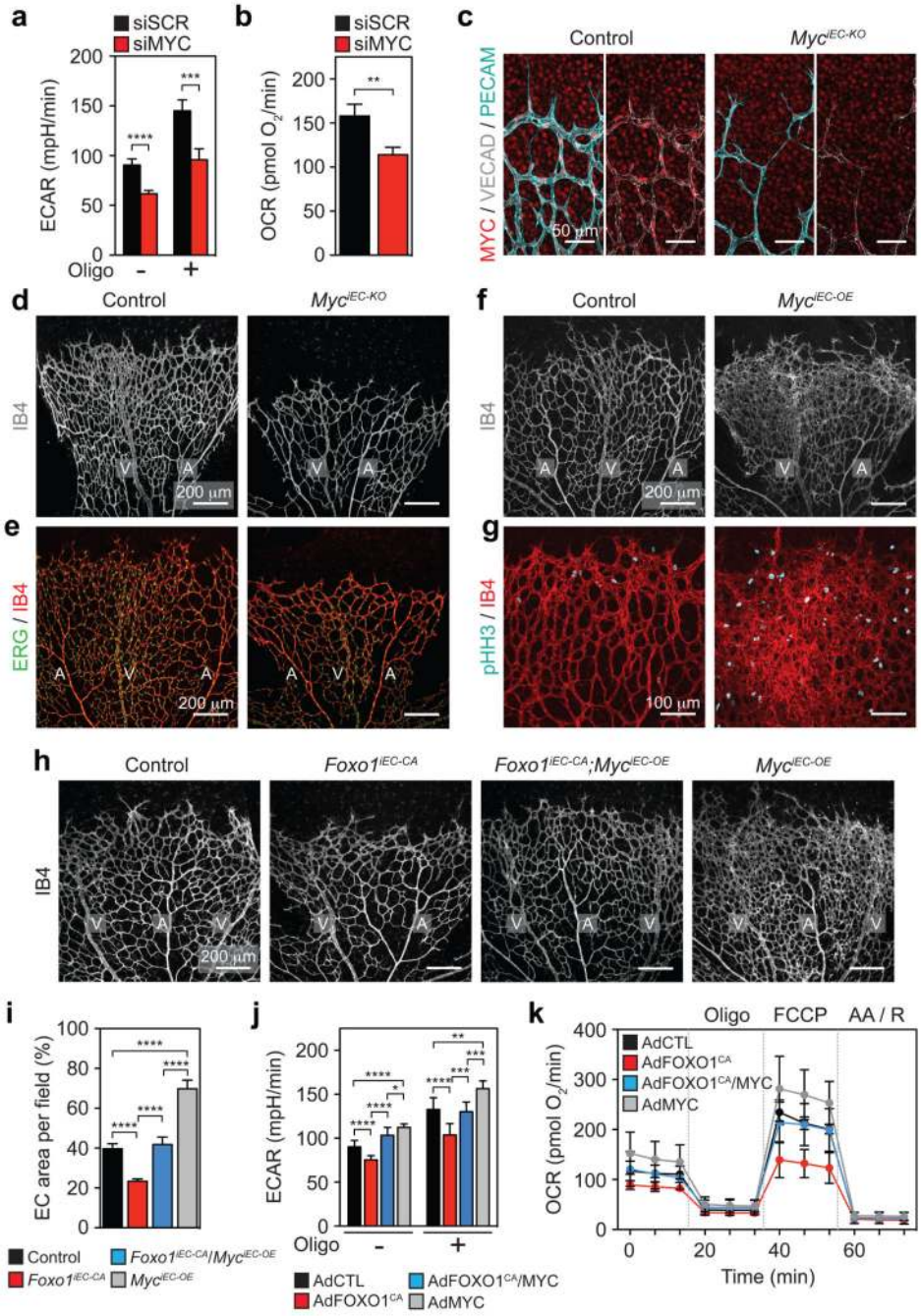

Figure 4. MYC is a critical component of FOXO1 signalling in ECs

a,b, ECAR (a) and OCR (b) in MYC siRNA- (siMYC) or scrambled siRNA- (siSCR) transfected ECs (ECAR: n = 5; OCR: n = 5). Data represent mean ± s.d., two-tailed unpaired *t*-test. **c**, Staining for MYC , VECAD and PECAM in retinas of $Myc^{iEC\text{-}KO}$ and control mice. **d**,**e**, Images of IB4- (d) and IB4- and ERG- (e) stained P5 retinas of control and $Myc^{iEC\text{-}KO}$ mice. **f**,**g**, Images of IB4- (f) and pHH3- and IB4- (g) stained P5 retinal vessels in $Myc^{iEC\text{-}OE}$ and control mice. **h,i**, Representative images (h) and quantification (i) of IB4-stained P5 retinas in control, $Foxo1^{iEC\text{-}CA}$, $Myc^{iEC\text{-}OE}$ and $Foxo1^{iEC\text{-}CA}/Myc^{iEC\text{-}OE}$ double

mutants (n ≥6). **j**,**k**, ECAR (j) and OCR (k) in AdCTL, AdFOXO1^{CA}, AdFOXO1^{CA}/AdMYC and AdMYC-transduced HUVECs showing restoration of metabolic activity in FOXO1^{CA}/MYC co-expressing ECs (ECAR: n = 8; OCR: n ≥3). Data in i-k represent mean ± s.d., one-way ANOVA with Bonferroni's multiple comparison post-hoc test. $^{**}P < 0.01$; $^{***}P < 0.001$; $^{****}P < 0.0001$.

Europe PMC Funders Author Manuscripts